# PROJECT FINAL REPORT

# Publishable summary

**Grant Agreement number: 310748**

**Project acronym: DRREAM**

**Project title: Drastically Reduced use of Rare Earths in Applications of Magnetocalorics**

**Funding Scheme: NMP Collaborative Project (Small)**

**Period covered: from 1/1/2013 to 31/12/2015**

**Name of the scientific representative of the project's co-ordinator, Title and Organisation:**

Karl G. Sandeman

Department of Physics

Imperial College London

United Kingdom

Tel: +44 207 290 9182

Fax: +44 207 594 2077

E-mail: k.sandeman@imperial.ac.uk

**Project website address: http://www.drream.eu**

**DRREAM**

Drastically Reduced Use of Rare Earths in Applications of Magnetocalorics

http://www.drream.eu



*DRREAM* partners at a project meeting in Dresden, June 2015

# 1. Executive Summary

*DRREAM (Drastically Reduced use of Rare Earths in Applications of Magnetocalorics)* was a 36-month project driven by a need to reduce the use of rare earths in future magnetic technologies. Magnetic cooling, the main focus of *DRREAM,* has been identified as a potential large-scale user of permanent magnets and of magnetic refrigerants that contain rare earth elements.

Magnetic cooling is a solid state cooling method that promises high system efficiency. It utilises the temperature change that occurs when a magnetic material is driven through a change of state by an applied magnetic field. Magnetic refrigerants have magnetic phase transitions around room temperature, just as HFCs evaporate readily at room temperature. However, they are solids and thus to not pose the same risks to the environment as volatile HFCs.

Our project was designed to bring together experts in material synthesis, production, theory, and engineering experts in domestic cooling and prototype magnetic cooling. The consortium's task was to improve magnetic refrigerant properties and the availability of thin plate, low wastage refrigerant morphologies so that the use of rare earths in the life cycle of a magnetic refrigerator could be reduced. A comparison was made of the design of an A+++ domestic refrigerator using the materials available at the beginning and at the end of the project. Our major achievements in *DRREAM* are now listed.

*Rare earth-containing, high magnetocaloric effect materials*

- Mechanically stabilised La-Fe-Si-based materials have been produced that enable plate production (see WP5) while maintaining excellent magnetocaloric properties
- A reduced annealing time route to single phase La-Fe-Si production has been identified: suction casting
- Thick films of La-Fe-Si have been made and future experiments will involve the deposition of such films on piezoelectric substrates
- The effect of shape on the dynamics and hysteresis of metamagnetic phase transitions in La-Fe-Si samples has been quantified.

*Efficient parts manufacture*

- Screen printing of La-Fe-Si-based materials was trialled, and binders were developed that optimise impurity concentrations after binder removal.
- Several production methods were investigated, including spherical particles and epoxy bonding
- An optimal method of production of magnetocaloric parts was selected for testing

*Rare earth-free magnetocaloric materials for magnetic cooling and power generation*

- Single phase Mn-Fe-P-Si materials were produced by a variety of methods and the correlation between grain size, preparation route and thermal hysteresis and the virgin effect was investigated
- Manganese borides were investigated for high temperature, thermomagnetic power generation properties
- FeRhPt films were produced on conventional and piezoelectric substrates

*Theoretical modelling*

- Ab initio models of several families of magnetocaloric materials (for cooling) and thermomagnetic materials (for power generation) were constructed
- Prediction of large piezomagnetism in Mn antiperovskites
- Agreement between thermodynamic models and experimental data on La-Fe-Si alloys
- Influence of inhomogeneities on Arrott plots was investigated

*Impact on rare earth use*

- Use of shaped La-Fe-Mn-Si-H regenerators delivers a 50% improvement in cooling performance over the baseline La-Fe-Co-Si material, without impacting efficiency (through achieving improved shaping of magnetocaloric parts, compared to the baseline design).
- Rare earth usage in the permanent magnets required for the original falls by 75% as a result
- Based on the final life cycle analysis (LCA), the total rare earth usage in an A+++ domestic cooler has fallen by 73%, when compared with the usage in the design at the start of the project.

Our ultimate goal was to lower the amount of rare earth material used in the life cycle of a future domestic magnetic refrigerator. Our prediction of a 73% reduction in RE usage, based on our optimised magnetic refrigerants, produced in thin plate form, is a result that we hope will propel magnetic refrigeration closer to commercialisation as a high efficiency, low carbon cooling technology.

# 2. Project context and objectives

## 2.1 Context

**The aim of our project has been to reduce the use of rare earth elements in technologies that use magnetic phase change materials.** Our primary focus was on room temperature magnetic cooling as a near-market solid-state alternative to gas compression refrigeration.

DRREAM was funded by the NMP-2012-4.4-3 call *Development of advanced magnetic materials without, or with reduced use of, critical raw materials* which was established as a result of heightened awareness of the importance of critical materials for future technologies. In particular, by 2011, it was anticipated that clean energy technologies and efficient energy use technologies would be expected to require an increasing fraction of the world's critical materials supply in the future[1]. By 2012, energy technologies already contributed to about 20% of the global consumption of critical materials[2], lists of which always contain rare earth metals and oxides. Neodymium (Nd) has been identified by the EC as being in the top 5 most critical materials for emerging technologies, when the forecast demand for 2030 is compared with that in 2006[3,4]. It was also listed by the DoE, along with dysprosium, in the top six most critical materials for clean energy technologies in the short term[2]. The same time period followed the rare earth crisis of 2009-11, during which the price of rare earth elements including Nd rose by up to 600% as a result of export restrictions in China.

Of the worldwide production of neodymium oxide, 69% typically goes to the manufacture of permanent magnets[5]. Meanwhile, lanthanum oxide constitutes 30% of rare earth oxide production worldwide. **However, assessments of materials criticality around 2011 often did yet include the impact of magnetic cooling** and of its demand for rare earth (Nd, Dy)-containing permanent magnets and potentially rare earth (La)-containing magnetic refrigerants, the working materials of a magnetic cooling cycle**.** We have therefore had a strong desire to minimise the use and eliminate wastage of both neodymium and lanthanum in the life cycle of a magnetic refrigerator.

Two other factors have increased the timeliness of magnetic cooling and an investigation into how to minimise its use of critical materials. The implementation of the European Union's WEEE (Waste Electrical and Electronic Equipment) and RoHS (Restrictions on the Use of Certain Hazardous Substances) directives requires cooling engine manufacturers to examine their current systems and look for alternatives with a lower environmental impact over the complete lifetime of the product. The net effect is that solid state cooling technology is attracting interest from all sectors and our work will enable manufacturers to comply with these regulations. Secondly, European Union directive EC C(2010) 6481 bans all domestic fridges lower than class A, and **created a new high-efficiency A+++ class from late 2011**. Consumer demand and the efficiency advantages of magnetic cooling will enable this directive to be followed.

**Magnetic cooling**

The magnetic cooling technique utilises temperature changes of solid magnetic refrigerants known as "magnetocaloric" materials, invoked by a magnetic field that is usually provided by a permanent magnet. We have addressed the fabrication, manufacture and use of the refrigerant, aiming to:

(1) reduce consumption and eliminate wastage of rare earths during the scalable manufacture of magnetocaloric parts; and

(2) drastically reduce the volume of rare earth permanent magnet through a step-change improvement in the performance of low-rare earth or rare earth-free magnetocaloric materials.

In what follows we use the term "magnetic refrigerant" and "magnetocaloric" interchangeably. This terminology is because a magnetic refrigerant relies upon the magnetocaloric effect (MCE), the change of temperature that a material undergoes when exposed to a change in applied magnetic field. In non-magnetic

[1] O. Gutfleisch et al., Adv. Mat. **23** 821-842 (2011).
[2] D. Bauer et al., U.S. Department of Energy Critical Materials Strategy (Dec. 2010).
[3] For Nd the ratio of 2030 to 2006 Emerging Technologies Raw Material Demand (ETRD) for Nd is 1.66 [3].
[4] European Commission, DG Enterprise and Industry, Critical raw materials for the EU: report of the Ad-Hoc Working Group on defining critical raw materials (2010).
[5] T.G. Goonan, Rare earth elements: End use and recyclability: U.S. Geological Survey Scientific Investigations Report (2011).

materials it is very small (hundredths of a Kelvin) but in materials that have a magnetic phase transition it can be as large as 3-4 K in a 1 Tesla field – a field easily achievable with a permanent magnet. The applied field can trigger the change of magnetic phase, and with it bring about a release or uptake of heat by/from the material. The amount of heat exchanged with the surroundings can be sufficient to build a cooling engine; in the best MCE materials, around 1 kW cooling power per kilogram of refrigerant might be expected.

For further description of the magnetocaloric effect, the magnetic cooling cycle, and the nature of the "regenerator" that is the functional unit of a magnetic *regenerator* that turns a single shot temperature change into a temperature span between the hot and cold ends of a device, we refer the reader to the Final report of the *SSEEC* available on cordis.europa.eu.[6] We note here two key properties of the magnetic refrigerant that are important in what follows:

- **When the magnetic field is applied isothermally (at a constant temperature) a large heat is released or taken in by the material (~ 10-20 J kg$^{-1}$K$^{-1}$). We quantify this in terms of isothermal entropy change, $\Delta S$.**
- **When the magnetic field is applied adiabaticaly (at constant entropy, or under conditions of no heat exchange with the material) a large temperature change is observed (~ 2 Kelvin in a 1 Tesla field change). We call this quantity the adiabatic temperature change, $\Delta T_{ad}$.**

Recent developments, notably in the *SSEEC* project[7] (NMP-FP7 CP-FP 214864, which involved many DRREAM partners) have demonstrated that we may expect cooling devices to use magnetocaloric materials in the next 3 years. The most often-considered room temperature MCE material until about 5 years ago was gadolinium, a rare earth element and strong ferromagnet with a Curie temperature of around 294 K. In the years to 2010, virtually all prototype magnetic cooling engines around the world used gadolinium metal as the working material.[8] The reasons were twofold: firstly cost and toxicity issues relating to the new generation of refrigerant materials and secondly an inability to produce large amounts of alternative magnetic refrigerants. Furthermore very few prototypes comprised more than a skeletal regenerator, the core component that acts as the replacement of the standard gas compressor. No magnetic cooling engine had been designed according to commercially-driven cost and power requirements.

In a European context, the situation changed in 2008, with the initiation of *SSEEC*. This 36-month NMP-CP programme addressed two issues: the identification of low cost magnetocaloric materials made from non-toxic elements and the design and integration of those refrigerants in the form of thin plates into a bespoke design of magnetic regenerator for application in a new kind of magnetic air-to-air heat exchanger. **The partnership for that project – which included 5 Partners from DRREAM – was the first to adopt a holistic approach to the construction of a high efficiency, cost- and performance-centred magnetic cooling engine.** All stages of design and build were integrated: magnetic materials synthesis (lab and bulk scale), characterization and modeling, permanent magnet design and build, and refrigeration systems manufacture (both at SME and major end-user levels).

*SSEEC* achieved several step changes that represent the state-of-the-art in their respective areas:

(1) a five-fold reduction in the cost per Watt of a magnetic cooling engine, particularly through minimisation of magnet volume;
(2) the development of powder metallurgical processes to produce thin plates of Co-doped La(Fe,Si)$_{13}$ refrigerant (hereafter La-Co-Fe-Si) with tuned transition temperatures;
(3) the integration of all necessary components into a working air-to-air heat exchanger
(4) a five-fold increase in efficient operation frequency during the project, with consequent reductions in the mass of permanent magnet required per Watt of output power.
(5) the first set of round-robin activities designed to identify sources of error in measurement of magnetocaloric materials;
(6) an investigation of novel processes (spin reorientation and artificial spin reorientation) by which the magnetocaloric effect might occur at the nano-scale.

[6] Final report - SSEEC (Solid State Energy Efficient Cooling), European Commission website http://cordis.europa.eu/publication/rcn/15828_en.html
[7] http://www.sseec.eu/
[8] B. Yu et al., Int. J. Refrigeration, **33,** 1029 (2010).

**Context detail I: Use of permanent magnets in magnetic cooling**

Items (1-4) arguably have the greatest impact on the speed of development of magnetic cooling. The first of these is the use of high-strength permanent magnets to drive the magnetic cooling cycle, inducing the magnetocaloric effect in the chosen refrigerant (item 1, above). We note that these magnets contain **30% Nd and ~1% Dy** by mass. They are therefore a focus for our attention when trying to reduce the consumption of rare earth materials in the magnetic cooling product. Design modularity between products will maximise recyclability while magnet design itself may have a small benefit for the mass of magnet used. However our aim within this project has been to reduce reliance on critical rare earths and so we have addressed how to further improve the cooling power/magnet mass ratio via **improvements in refrigerant performance that will bring about the greatest permanent magnet utilisation.**

**Context detail II: Manufacture of magnetocaloric parts**

Magnetic cooling engines require magnetocaloric structures known as *regenerators* that are sufficiently thin to allow for efficient heat exchange with a suitable fluid. The *SSEEC* project was the first to make such parts for a cost-centred end-use application, and importantly the first to consider how to control the shape changes that can occur around the magnetocaloric material's phase transition. Figure 2.1 shows the results of item (2) in the above list: a range of plates of the active magnetocaloric material, La-Co-Fe-Si used in the *SSEEC* prototype, with thicknesses down to 0.25 mm. These plates were produced in SSEEC by a multi-stage route involving powder metallurgical formation of the desired composition, thermal decomposition ("TD") into a phase that is easier to cut, cutting to the required dimension (electrical discharge machining, EDM) and a final "recombination" ("R") heat treatment to bring back the desired, active magnetocaloric phase. The so-called "TDR" process was fully exploited during *SSEEC* and is unique to the metallurgy of $La(Fe,Si)_{13}$ and its alloys[9]. The plates produced were the thinnest made at that time for magnetocaloric research. We note that these plates **contained ~17% Lanthanum by mass**.

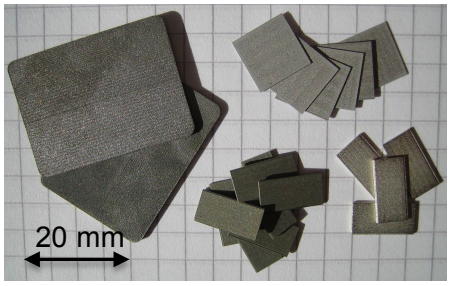


**Figure 2.1:** Plates of La-Co-Fe-Si produced in SSEEC (2008-2011) by the TDR process, cutting and heat treatment. A wide variety of thicknesses were made.

Due to large magnetovolume effects, **conventional manufacturing methods for metal parts do not allow cost-effective manufacturing of large quantities of such thin pieces of material**. The above work on 250 $\mu$m-thickness plates of La-Co-Fe-Si demonstrated their manufacturability on a small scale, but also the difficulties associated with handling functional materials that undergo a volume change related to their magnetic transition. Volume changes can be problematic during the machining of parts, resulting in bending or warping. The TDR process described above enabled the machining of hundreds of parts that are then cut using wire EDM. However, such cutting is very time-intensive and **up to 80% of the starting material is wasted**. **Since the parts contain ~17% lanthanum, it is imperative to optimise their efficient manufacture.** The shapes of current regenerator forms were limited by manufacture methods and we explored a variety of manufacture approaches in DRREAM.

**Context detail III: Rare earth-free magnetocaloric materials**

As outlined above, the rare earth element gadolinium (Gd) has been the refrigerant of choice for many magnetic cooling engine prototypes, due to its relatively large cooling effect and simplicity of production. However, the cost of high purity material, in which the best magnetocaloric effects are observed, is prohibitive. It is worth restating the properties of a good magnetocaloric refrigerant required for application, namely:

- a sharp magnetic phase transition that can be tuned by compositional changes across the room temperature range
- the phase transition can be induced at fixed temperature in the applied magnetic field of a simple permanent magnet (~1 Tesla)
- large magnetic moment
- low phase transition hysteresis (thermal and magnetic)
- metallic thermal conductivity (1-10 $Wm^{-1}K^{-1}$)
- moderate heat capacity

[9] M. Katter et al., Proceedings of the 4th International Conference on Magnetic Refrigeration at Room Temperature (Baotou, China August 2010), Ed. P. Egolf et al. (IIR, Paris)

In the last 10 years, two material families have emerged that have a low rare earth content. The first, LaFeSi, was the primary subject of applied study in *SSEEC* and developments beyond state-of-the-art in the entropic response and in the manufacture of plates will most quickly accelerate magnetocaloric material applications. As stated above, it contains 17% La by mass. The second, $(Mn,Fe)_2(P,Z)$ where Z=Si,As or Ge is less explored in published studies of magnetocaloric material deployment in cooling engines and is of commercial interest[10]. The observation of large magnetocaloric effects in this rare earth-free system highlights the interest in searching for rare earth-free magnetocaloric materials.

Rather than bulid a series of cooling engines, the *DRREAM* project has made advances in the magnetocaloric properties of materials, and in the manufacture of parts with thin dimensions, in order to be able to predict future reductions of RE use in a domestic magnetic cooling device. Our principal objectives are outlined in the next section.

## 2.2 Objectives

The deployment of the magnetocaloric effect requires two kinds of magnetic material:

(1) The “active” magnetocaloric material, which undergoes a phase change, and
(2) The permanent magnet[11] used to induce that phase change.

As described above, legislative and consumer pressure and advances in prototyping make magnetic refrigeration the most desirable future method of cooling at room temperature. State-of-the-art magnetocaloric and permanent magnet materials both currently contain some rare earth elements. As a result, magnetic cooling has been identified by the US DoE[12] and the Öko Institute[13] as a sector that will increase our consumption of rare earths in the medium term. Our research focussed on **the magnetocaloric material** and has enormous potential to reduce rare earth use in both (1) and (2) above. Specifically, we brought together a consortium experienced in both magnetic materials research and industrial scale manufacturing to:

a) achieve a step-change in the performance of La-containing magnetocaloric alloys;
b) explore high magnetocaloric effect, non rare-earth containing alloys for magnetic cooling
c) minimise wastage in the manufacture of magnetocaloric parts, through near-net shape manufacture including 3D screen-printing.
d) achieve a reduction in the volume of permanent magnet required in cooling applications, through (a) and/or (b) and/or (c)
e) exploit the knowledge we gain to accelerate parallel technologies including thermomagnetic power generation and energy-harvesting micro-systems.

**By the project completion date we achieved a 73% reduction of the use of RE in a model of an A+++ magnetic refrigerator, based upon our advances in magnetocaloric properties and manufacturing techniques. We also explored the microstructure-function relationship in a number of magnetocaloric materials, and made added-value discoveries, including that of giant piezomagnetism in Mn-based antiperovskites.**

[10] F. Seeler, G. Degen, B. Reesink and J. Kaczun, Patent application WO/2010/108883 (2010).
[11] The use of an electromagnet is not considered here, on efficiency grounds.
[12] D. Bauer et al., U.S. Department of Energy Critical Materials Strategy (Dec. 2010).
[13] D. Schüler et al., Study on rare earths and their recycling, (Öko-Institut e.V., Jan. 2011).

# 3. Main S&T results and foregrounds

### Structure

Our magnetocaloric material selection is based on both the need to provide a step change in performance and manufacturability for rapid technological development and the desire to obtain new knowledge of functional phase change materials. Therefore, such materials were explored in three parallel strands that correspond to work packages (WPs) 1, 2, and 3. Theoretical modelling was applied to a number of materials and corresponded to WP4. The impact of our materials innovations was judged by comparing life cycle analyses of a future magnetic fridge design at the start of the project with that at the end (WP5).

In Figure 3.1 we show the life cycle of a magnetic refrigerant, together with the impact of our programme on the consumption of rare earths (REs) at each stage. From Figure 3.1 we can see that there is scope for significant reduction of rare earth consumption in three ways that address each of the challenges outlined above. Our work required a consideration of all relevant steps and impacts both of the rare earth-containing components in magnetocaloric devices: the active material and the permanent magnet used to drive it.

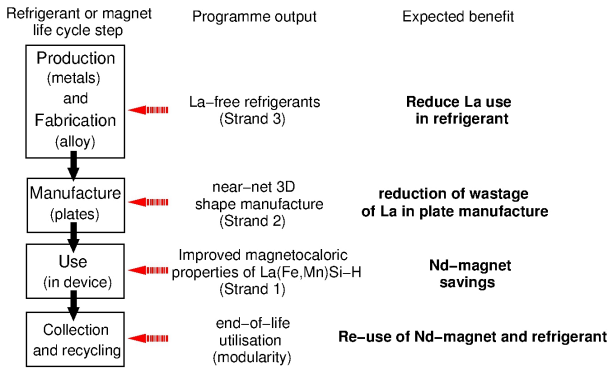


**Figure 3.1:** Schematic life cycle for magnetocaloric refrigerants. Main processes are on the left. Our impact on different stages of the life cycle are indicated in bold on the right. After Graedel et al.[14].

In the following subsections we present a selection of research highlights, organised in work package (WP) order. Full details are given in the technical annexe accompanying this report. The WPs were:

- WP1: Rare earth-containing, high magnetocaloric effect materials
- WP2: Efficient parts manufacture
- WP3: Rare earth-free magnetocaloric materials for cooling and power generation
- WP4: Theoretical modelling
- WP5: Impact on rare earth use
- WP6: Consortium management (administrative)
- WP7: Scientific management (RTD)
- WP8: Networking activities, dissemination and exploitation

There was a strong degree of inter-relation between research activities in the different WPs. This was crucial to the project. Single phase bulk La-Fe-Si-based materials produced in WP1 were produced in different morphologies in WP2. The manufacture of some rare earth-free WP3 materials was also explored using production routes in WP2. Data on bulk compounds in both WP1 and WP3 was used as the basis for theoretical modelling at various length scales in WP4. Predictions from WP4 modelling also acted as the stimulus for further experimentation in WP1 and WP3. The best data from WP2 were used to select materials for analysis under WP5. An initial life cycle analysis (LCA) was made in WP5 and updated using the results available at the end of the project.

[14] T.E. Graedel et al., Journal of Industrial Ecology **15** 355 (2011).

## 3.1 WP1: Rare earth-containing, high magnetocaloric effect materials

**Objectives**

- To establish single phase compositions of La-Fe-Si-H magnetic refrigerants with large field-induced entropy changes, low hysteresis and tuneable critical temperatures for manufacture in parts.
- To establish new and optimised routes to synthesis of single phase powder of such materials.
- To make thick films of La-Fe-Si for control via piezoelectric substrates.
- 80% improvement in entropy change of substituted single-phase alloys compared to La-Fe-Co-Si at room temperature

**Summary of activities**

WP1 used Lanthanum-containing iron alloys that had been shown to have good magnetocaloric properties. La-Fe-Si possesses an abrupt, "first order" magnetic transition that can be tuned to room temperature by the addition of cobalt (which reduces the first order nature) or by the absorption of hydrogen (which maintains the first order nature). Our aim was to improve the performance of low-rare earth magnetocaloric LaFeSi by moving from Co doping to co-substitution of Mn and H, and thereby increase efficiency and reduce magnetic field need. Our intention was to yield an almost twofold **improvement in the entropic response of these materials,** and so bring about a drastic reduction in the volume of rare earth permanent magnet used to drive them in application. **This aim was fully achieved.**

Initially, Co-doped materials with second order magnetic transitions were studied from the point of view of production. Around 70 kg of La-Fe-Si material was produced in powder form, for use in WP2 and WP5. Latterly, Mn/H-doped first order materials were delivered in bulk quantities for manufacture into parts. It is the latter materials that possess the highest MCEs.

Thick films of La-Fe-Si were produced by CNRS-Néel in order to study combinatorial composition effects and the possibility of driving the material by an external electric field (via a piezoelectric substrate). Films were produced and the reproducibility of their production was investigated.

Regarding material synthesis, vacuum casting was developed as future method of La-Fe-Si synthesis that requires only short anneal times. Lastly, the dependence on material shape of the nucleation of the field-induced metamagnetic transition in first order La-Fe-Si alloys was investigated.

### 3.1.1 Highlights of La-Fe-Si activities

The highlights presented in this section are arranged under three headings:

- 80% enhancement of magnetocaloric effect in Mn/H doped alloys
- Reduced annealing times in suction cast alloys
- Thick films of La-Fe-Si produced for the first time
- Dynamics of metamagnetism in La-Fe-Si investigated with a view to hysteresis minimisation

*80% entropy enhancement in single phase La-Fe-Si-based alloys (VAC)*

This milestone was fully achieved with mechanically stabilized La-Fe-Mn-Si-H alloys. Figure 3.2 shows the entropy change of this alloys compared to La- Fe-Co-Si. Mechanically stabilized La-Fe-Mn-Si-H exhibit about 80% higher entropy change compared to La-Fe-Co-Si around room temperature. A major achievement is the fact that the two alloys can be prepared in the same final shape and therefore a direct comparison is valid.

The parent La-Fe-Mn-Si-H alloy has an even higher entropy change but can only be prepared as granulate material, which can be arranged in the form of packed bed regenerators. However such packed bed regenerators suffer from large pressure drops. The pressure drop counteracts the positive effects which come from the higher entropy change. The flat plate regenerator structures studied in WP2 and WP5 do not suffer from such significant pressure drop problems.

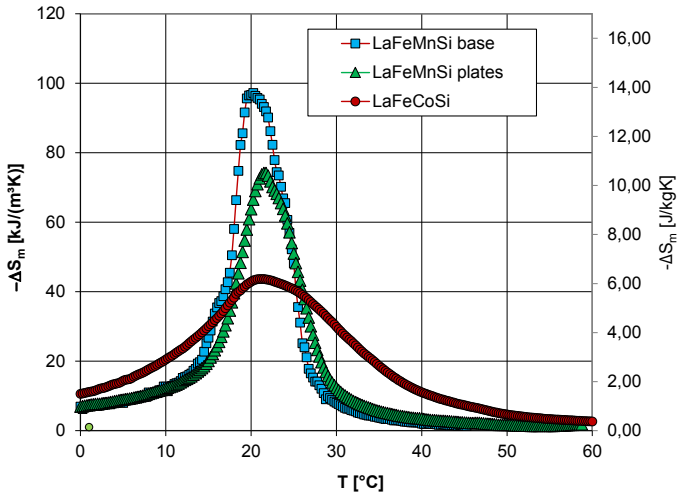


**Figure 3.2:** Magnetic entropy change of LaFeCoSi compared the $LaFeMnSiH_x$, showing the 80% entropy enhancement that could be achieved through substitution of Mn for Co and through hydrogenation.

*Reduced annealing times in suction cast alloys (TU Darmstadt)*

$La(Fe,Si)_{13}$ alloys are a good candidate as the active, magnetocaloric material in a cooling device, due to their high MCE properties which only occur in the 1:13-phase. To reach a high phase purity of 1:13-phase in conventional methods, high temperatures, long annealing times or greater effort (such as milling) are required. As the formation of 1:13 phase is kinetically hindered in bulk samples, long annealing times in the range of several days are needed. Melt spinning has been shown to be a viable option to produce large amounts of 1:13 phase with short annealing times.

TU Darmstadt established a suction casting production technique in order to prepare (nearly) single phase material with a high phase ratio of the 1:13 phase.

The suction casting setup used was a modification of a conventional arc melter system. The basic principle of suction casting is simple. First, the material to be suction cast has to be placed to a water-cooled copper plate. The copper plates used in our experiments have different types of channels for different geometries and different cooling rates. Two samples of the used copper channels are shown in Figure 3.3 (left and middle images). The working principle of the suction casting can be explained in the following way. First, the material is melted with the arc and the resulting liquid metal is casted in to the water-cooled copper bore with the help of the vacuum. The schematic representation of the setup is shown in Figure 3.3 in the image on the right hand side.

By choosing the shape of the suction channels heat exchangers can be shaped into many different shapes like rods and plates directly.

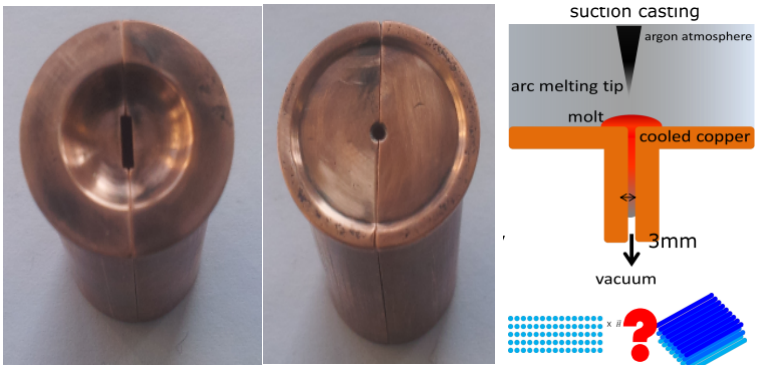


**Figure 3.3:** (left) Copper suction casting crucibles with different suction channels. (Right) working principle of suction casting showing the possibility of producing heat exchanger geometries directly from the melt.

The adiabatic temperature change measurements of both the suction cast and induction melted samples are shown in Figure 3.4. The adiabatic temperature change was directly measured in a home built setup where magnetic field changes up to 1.9 T can be applied. The suction cast sample displays an adiabatic temperature change ($\Delta T_{ad}$ ) of approx. 6 K, whereas the induction melted samples shows a $\Delta T_{ad}$ of "only" 5 K. This fact can be attributed to the higher amount of magnetocalorically active 1:13 phase in the suction casted sample compared to the induction melted sample.

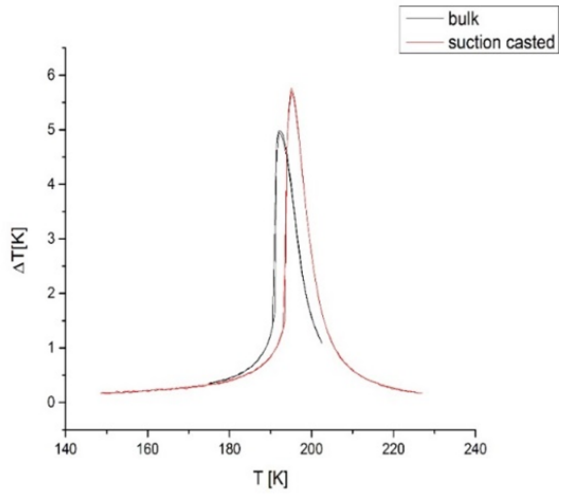


**Figure 3.4:** Adiabatic temperature change of $La(Fe,Si)_{13}$ produced via induction melting (bulk) and suction casting after annealing

In conclusion, suction casting is a valid alternative approach for preparing large scales of high performance $La(Fe,Si)_{13}$ in an economic way. The annealing time of the suction cast samples can be reduced by one order of magnitude with only a slightly higher annealing temperature compared to the conventional induction melting approach. As diffusion is a function of time and diffusion parameter (which is a function of temperature), changing the thermal treatment condition and timespan allows us to tune the diffusion properties of the investigated system. In this project, it was shown that the microstructure of the main La-Fe-Si phase and secondary phases could be modified (not shown in this report). After suction casting we obtained a finer microstructure of the secondary phases and this results a significant reduction in the diffusion lengths. By reducing the diffusion lengths and increasing the diffusion parameters with a slight increase of the thermal treatment condition we managed to reduce the annealing time significantly.

After optimized annealing the resulting samples show a high homogeneity of the microstructure and quite a low amount of secondary phases. In addition, one can produce near-net-shape heat exchanger geometries by using the suction casting method which will reduce the secondary machining for shaping. With this approach it is possible to reduce the amount of raw material wastage which can result from shaping.

*Thick films of La-Fe-Si (CNRS-Néel)*

Studies to date of the $La(Fe,Si)_{13}$-system have focused on bulk alloys, with no reports on $La(Fe,Si)_{13}$ in film form. Thin and thick films may serve as model systems for materials studies and also have potential for use in micro-systems. CNRS Grenoble proposed to study the preparation of $La(Fe,Si)_{13}$ in film form, using a combinatorial approach in which compositionally graded films are deposited on large substrates. A first study concerned magnetron sputtering of relatively thin films ($t \leq 350$ nm) using a composite target consisting of a base of pure Fe and superposed pieces of La and Si. This target geometry was chosen to maximise the composition spread, which was dependent on both the size and position of the superposed elements.

Figure 3.5 shows room-temperature XRD patterns for these 5.3 $\mu$m-thick La-Fe-Si films after post-deposition heat treatment at 1073 and 1173 K. It can be seen that the La-Fe-Si films crystallize in the $NaZn_{13}$-type cubic structure. Additional diffraction peaks are attributed to alpha-Fe, a La-rich phase, $Fe_7Ta_3$ and Fe-containing βTa. The formation of the latter two phases, due to diffusion between the main layer and the buffer and

capping layers during the annealing process, is supported by a literature report on the binary Ta-Fe systems[15]. No $NaZn_{13}$-type phase was detected after annealing below 973 K (data not shown).

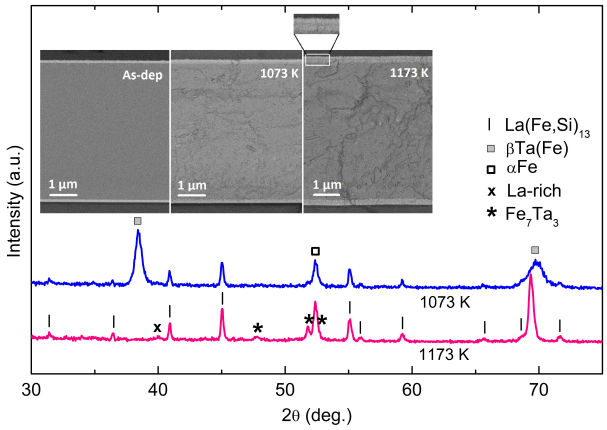


**Figure 3.5:** Room temperature XRD pattern for 5.3 $\mu$m thick La Fe Si films after annealing at 1073 and 1173 K. The inset shows cross-sectional backscattered electron SEM images for the La-Fe-Si films before (left) and after annealing at 1073 (middle) and 1173 K (right).

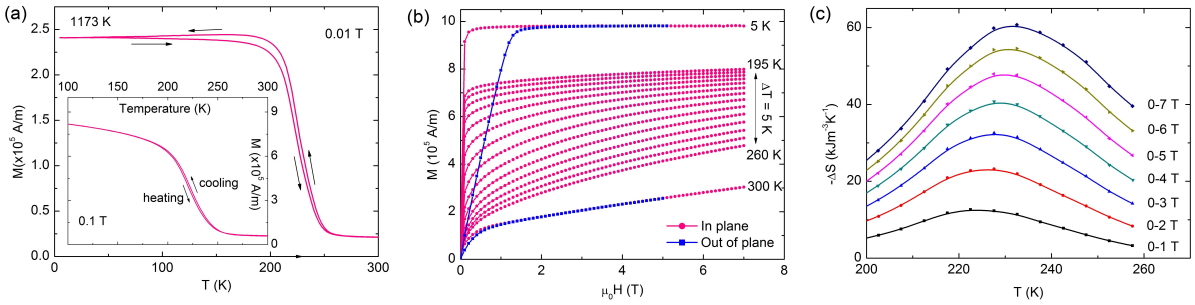


**Figure 3.6:** (a) Temperature-dependent magnetization on cooling and heating measured in the in-plane direction in magnetic fields of 0.01 T and 0.1 T (inset); (b) the magnetization as a function of magnetic field in the in-plane and out-of-plane directions; and (c) the isothermal entropy change under field changes in the vicinity of $T_C$ for the La-Fe-Si films after annealing at 1173 K.

Considering the La-Fe-Si films before and after annealing at 1173 K, EDS analysis conducted on the as-deposited and annealed films indicate compositions of $LaFe_{11.2}Si_{1.9}$ and $LaFe_{10.9}Si_{2.1}$, respectively. This change in composition may be attributed to the diffusion of Fe into the Ta layers. The lattice constant at room temperature (a = 11.456 Å) of the annealed $LaFe_{10.9}Si_{2.1}$ films derived from XRD analysis is very close to that reported for bulk alloy of the same composition.[16,17] Figure 3.6(a) shows magnetization as a function of temperature in a field of 0.01 and 0.1 T measured in the in-plane direction for the La-Fe-Si film after annealing at 1173 K. A broad transition from the paramagnetic to the ferromagnetic state suggests a second-order magnetic phase transition with $T_C$ = 245 K. Having succeeded in preparing $La(Fe,Si)_{13}$ in film form, future deposition of such films onto piezoelectric substrates so as to study the influence of strain on the film's M(T) transition characteristics.

*Dynamics of metamagnetism; the impact of material shape on magnetic hysteresis (Imperial)*

In this study we examined the dynamic properties of $La(Fe,Si)_{13}$ based samples showing that the magnetic hysteresis could be engineered unexpected by sample shape. A sample of 2mm x 1mm by 0.4 mm geometry was cut into three parts. Sample A was the original complete sample, sample B was the sample cut into three parts but pressed together into the original shape to retain the same global demagnetization and sample C, was the three parts well separated.

[15] V.T. Witusiewicz, A.A. Bondar, U. Hecht, V.M. Voblikov, O.S. Fomichov, V.M. Petyukh, and S. Rex, Intermetallics **19,** 1059 (2011).
[16] B.G. Shen, J.R. Sun, F.X. Hu, H.W. Zhang, and Z.H. Cheng, Adv. Mater. **21,** 4545 (2009).
[17] K. Niitsu, S. Fujieda, A. Fujita, and R. Kainuma, J. Alloys Compd. **578,** 220 (2013).

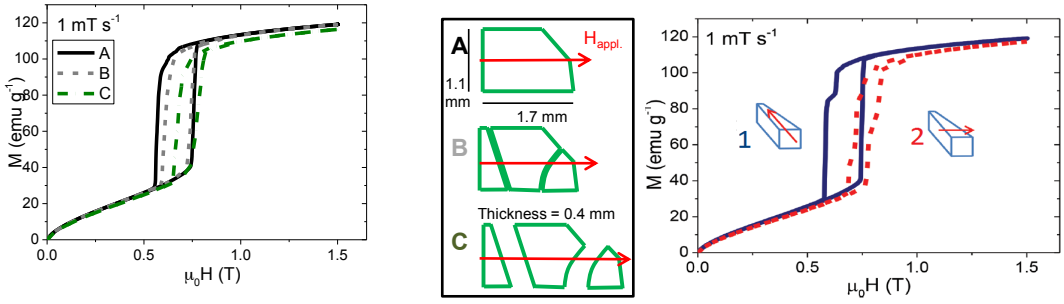


**Figure 3.7:** Shaping of parts for first order $La(Fe,Si)_{13}$ compounds can take advantage of the non-obvious role of geometry to reduce the effective magnetic hysteresis.[18]

Figure 3.7 shows the *M-H* loops for the three samples A, B, and C showing that the paramagnetic to ferromagnetic transition field $H_{c1}$ is similar for all three samples, but the ferromagnetic to paramagnetic transition is strongly affected by sample geometry. For materials with a sharp first order transition, the first region of the sample to nucleate the ferromagnetic phase is the area of the sample where the local field is high, and for the reverse transition the first region to nucleate the paramagnetic phase is where the local field is low. This is the origin of the effect. To further illustrate that this is counter intuitive the right hand panel of Figure 3.7 shows the hysteresis loop along the short bar shaped sample and in the plane but perpendicular to it. It is the latter geometry that yields the lowest hysteresis loop. This shows that for materials with sharp first order transition and magnetoelastic coupling, sample shape effects can dominate in interesting ways, potentially important for application.

### 3.1.2 Conclusions of WP1

In summary, the main results of work in WP1 are:

- Mechanically stabilised La-Fe-Si (LFS) materials have been produced that enable plate production (see WP5) while maintaining excellent magnetocaloric properties
- A reduced annealing time for phase La-Fe-Si production via suction casting
- Thick films of La-Fe-Si have been made and future experiments will involve the deposition of such films on piezoelectric substrates
- The effect of shape on the dynamics and hysteresis of metamagnetic phase transitions in La-Fe-Si samples has been quantified.

## 3.2 WP2: Efficient parts manufacture

### Objectives

- To develop a binder for the production of magnetocaloric parts by 3D-screen printing
- To investigate binder development for RE-free magnetocaloric parts
- To produce a range of non-screen-printed morphologies of La-Fe-Si-based parts for testing

### Summary of activities

This second strand explored manufacturing methods including state-of-the-art 3D screen-printing, to enable near-net shape manufacture of material parts for cooling engines. The Lanthanum-containing iron alloys of the first strand, WP1, were the primary subjects for study. Our aim was a **fourfold reduction in the rare earth (Lanthanum) wastage normally associated with the cutting of parts** from alloy blocks. All aspects associated with the manufacturing of shapes by screen-printing – binder selection, heat treatment, and the feedback between manufacturing process and functional property – were examined. The performance of parts in the project were benchmarked in test structures within WP5.

[18] E. Lovell, A.M. Pereira, D. Caplin, J. Lyubina and L.F. Cohen, Advanced Energy Materials **5,** 1401639 (2015).

### 3.2.1 Highlights of screen printing activities

The highlights presented in this section are arranged under two headings:

- Binder development
- Printing studies

A modified 3D-screen-printing process was developed by Fraunhofer using refrigerant powders produced by Vacuumschmelze in order to manufacture thin plate-like parts. For this purpose, a powder-binder mixture has to be printed layer-on-layer to the desired shape followed by a conventional sintering step. The advantage of a 3D-screen-printing process lies in the possibility to manufacture complex designs including fine walls, such as required in multi-channel regenerators. Furthermore, 3D-screen printing is fast, highly cost effective and ideally suited for mass production.

The key to the technology is the formulation of the printable paste containing a (often water-based) binder system and the powder to ensure the stability and the shape of the manufactured "green part". After printing the structures are heat treated to remove the binder and sinter the powder. For the binder removal the process has to be adapted to the particular binder system / powder combination to avoid any contamination by residual oxygen and carbon, which would degrade the materials properties. For this purpose an IR-spectroscopy technology is used to determine the optimal heat treatment parameters. With this combination of printing technology, binder knowledge and optimised heat treatment it has been possible in the past to manufacture parts of different materials based on steel, nickel, titanium, molybdenum, tungsten, copper and ceramics[19].

*Binder development*

Processing of rare earth-containing La-Fe-Co-Mn-Si powder requires the development of a processing route which guarantees low oxygen, nitrogen and carbon contaminations. Otherwise oxygen and nitrogen impurities will form oxides and nitrides with Lanthanum, thus reducing the amount of Lanthanum forming an actually magnetocalorically active phase. The control of carbon ensures a reliable tuning of Curie temperature (Tc). However, nitrogen and oxygen as well as carbon are introduced into the material system when applying 3D screen printing since the printing paste needs organic substances in order to adjust viscosity (viscosity modifiers) and to provide binding force (binder) between metal particles in the green state.

A promising mixed binder formulation was devised by IFAM. Debindering tests at VAC were carried out, and a promising paste was developed based on those results. However, the binder combination resulted in a different debindering behaviour as the isolated substances. The contamination levels for O,C and N were hence high but screen printing was carried out to demonstrate the feasibility of manufacturing screen printed parts of La-Fe-Si-based material.

An alternative binder substance was introduced by VAC and it was found that this binder can be easily thermally debindered from VAC's La-Fe-Co-Mn-Si-powder. A new paste was also formulated, based on the binder selected by VAC. Stencil printing (which allows for plates to be prepared in a single run) was set up and a suitable thickening agent, that was O- and N-free was identified.


**Figure 3.8:** Plates of La-Fe-Co-Si prepared with the first binder recipe.

[19] P. Quadbeck, B. Schreyer, A. Strauß, T. Weißgärber, B. Kieback, Proc. Powder Metallurgy World Congress & Exhibition. PM2010, Florence, Italy 10-14 October 2010, Vol. 2, pp. 239-245

*Printing studies*
Using one of the first binder mixture, screen printing machine parameters were identified in order to avoid frequent screen breakage. An appropriate heating cycle was found. Paste drying-induced warpage was also overcome. Samples of the such prepared plates can be seen in Figure 3.8. Debindering of these plates is the subject of further study.

### 3.2.2 Highlights of non-screen printed production methods

The highlights presented in this section are arranged under two headings:

- Polymer (epoxy)-bonded heat exchangers
- Magnetocaloric spheres
- Other methods

*Polymer-bonded heat exchangers (TU Darmstadt)*
Heat exchangers consisting of polymer-bonded $La(Fe,Si)_{13}$ were fabricated and their magnetocaloric properties studied. It has been shown that the magnetocaloric effect can be tailored by compacting magnetocaloric powder with epoxy. Compaction with epoxy allows improving the mechanical integrity and thermal conductivity of the compacted samples. There are many variables such as type of epoxy, compaction pressure, epoxy to powder ratio. It was found that the adiabatic temperature change $\Delta T_{ad}$ of the polymer-bonded plates is 10 % higher than for the initial bulk material. A critical value for the compaction pressure of 0.1 GPa was found. Exceeding this value leads to a drastic reduction of the magnetocaloric effect due to cracking of the initial 50-100 $\mu$m grains down to fragments of 1-10 $\mu$m. Different types of epoxy were tested. A thermally conductive silver epoxy was found to yield the highest values of adiabatic temperature change. Figure 3.9 (left) compares the adiabatic temperature change for a field sweep of 1.9 T for $LaFe_{11.6}Si_{1.4}$ bulk (solid line), 100 $\mu$m powder compacted under 0.1 GPa (dashed line) and of powder mixed with 5 wt % silver epoxy compacted under 0.1 GPa (dashed-dot line). The compacted powder shows a higher $\Delta T_{ad}$ compared to bulk. This is attributed to constraints effects. Despite the slight dilution of the material, an increase in $\Delta T_{ad}$ of the powder-epoxy compared to the compacted powder is observed.

Thin plates of 0.6 mm thickness were fabricated using $LaFe_{11.6}Si_{1.4}$ powder with 5 wt % of silver epoxy and compacted under 0.1 GPa. These plates were assembled into a simple porous heat exchanger with straight 0.6 mm-width channels. Subsequent work involved a comprehensive optimisation of the magnetocaloric properties and the mechanical integrity of polymer-bonded $La(Fe,Mn,Si)_{13}H_x$ powder from VAC, by varying:
(1) the particle size,
(2) the compaction pressure,
(3) the amount and
(4) the type of epoxy adhesive.

The magnetic entropy change $\Delta S_m$, the adiabatic temperature change $\Delta T_{ad}$ and the heat diffusivity α were used for an assessment of the magnetocaloric properties of the composite material.

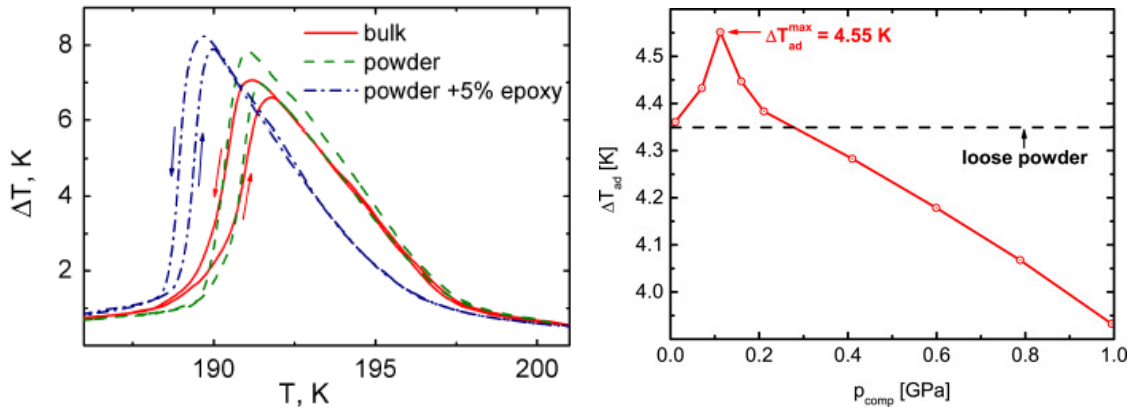


**Figure 3.9:** Left: Measurements of adiabatic temperature change (0 to 1.9 T) for bulk and compacted powder. Right: Adiabatic temperature change of compacted powder $La(Fe,Mn,Si)_{13}H_x$ samples, prepared from powders with a particle size of 160–250 µm.

The full results demonstrate advantages and the functional range of $La(Fe,Mn,Si)_{13}H_x$ composites in comparison with bulk $La(Fe,Co,Si)_{13}$ alloys and Gd metal and are published in Radulov et al.[20]

Three series of samples were prepared from this $La(Fe,Mn,Si)_{13}H_x$ material. Series 1 consisted of non-compacted loose powder samples; series 2 was compacted at 0.01–2 GPa without any glue or epoxy, whereas series 3 was manufactured as cold-compacted polymer-bonded composites. All samples were prepared as parallelepiped pellets with a base of 5×10 $mm^2$ and thickness of 1–3 mm depending on the preparation method. All samples were produced with a mass of 700 mg. Series 1 was prepared by tightly packing the powder in paper weighing boxes. Series 2 and 3 were compacted in a special designed toolset, which consisted of two punches and a disassembled die.

In order to select an appropriate binder for series 3, initially 7 different epoxy adhesives (thermoconductive, insulating, etc.) were used to prepare polymer-bonded samples. The two most appropriate epoxy adhesives were selected by $\Delta T_{ad}$ measurements on those samples. The samples from series 3 were produced using only these two adhesives: the thermal conductive silver based epoxy *H27D* (further referred as epoxy 1) produced by EpoTek Inc with a thermal conductivity of 1.2 $W^{-1}K^{-1}$ and a density of 3.5 g $cm^{-3}$, and the *Epoxyharz L* (further referred as epoxy 2) from R&G Faserverbundwerkstoffe with a thermal conductivity of 0.4 $Wm^{-1}K^{-1}$ and a density of 1 g $cm^{-3}$.

The influence of the compaction pressure on the magnetocaloric properties was investigated by measuring the $\Delta T_{ad}$ of rectangular shaped pellets prepared from 160 to 250 µm powder. The compaction pressure was increased from 0.01 to 2 GPa (series 2). The experimental $\Delta T_{ad}$ dependence on compaction pressure presented in Figure 3.9 (right) as a pronounced maximum at 0.1 GPa and decreases monotonically with increasing pressure in the range 0.1–2 GPa.

In summary, the optimal results were obtained with a particle size larger than 200 µm, a compaction pressure of 0.1 GPa and approx. 5 wt.% of low viscosity epoxy adhesive with a density of 1 g $cm^{-3}$ or less in order to obtain a polymer-bonded $La(Fe,Mn,Si)_{13}H_x$ composite with optimal magnetocaloric properties. Further experiments performed on polymer bonded samples are published in TUD's study.[21]

*Magnetocaloric spheres (VAC)*

As a method to produce spherical material fluidized bed granulation was investigated by VAC. The principle of the process is shown in Figure 3.10. A suspension of the desired material, binder, and solvent is sprayed through a nozzle into a vessel. At the same time, heated inert gas is blown into the vessel which dries the solvent and leaves the binder and metal powder behind. The binder leads to agglomeration of powder particles. If the processing parameters are chosen correctly the spherical particles are built up by a continuous fluidized bed. Possible particle sizes are in the range of 300 – 1000 *µ*m which is compatible to the requirements needed for efficient magnetocaloric regenerators. Regarding contamination from organic binders the same restrictions that apply to 3D screen printing apply to fluidized bed granulation. However, a suitable binder was found which can be debindered well without compromising the magnetocaloric properties of the sintered spheres.

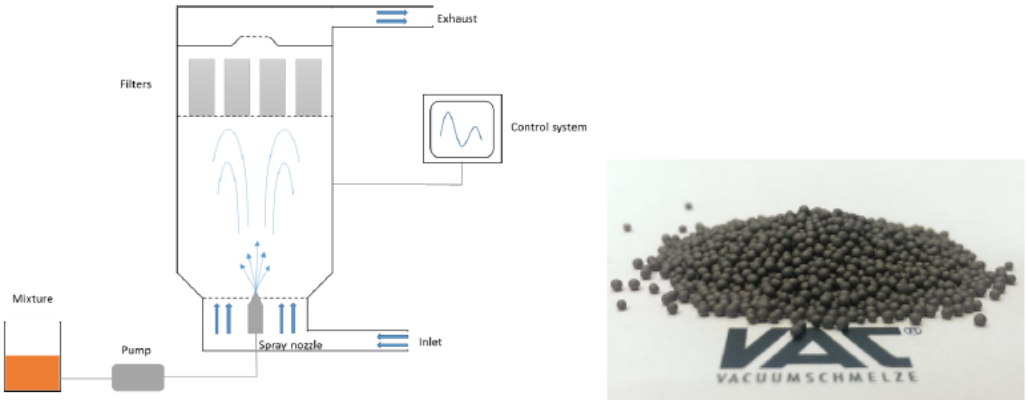


**Figure 3.10:** Left: Schematic drawing of fluidized bed granulation used to prepare “green” state spheres. Right: Sintered spheres.

[20] I. Radulov et al., JMMM **396,** 228 (2015).
[21] Radulov et al., IEEE Trans. Mag. 51 (2015), p 2501204

*Other methods*
In addition to the methods outlined above, other methods of part production were trialled in order to obtain the thinnest possible, magnetocalorically active plates.

### 3.2.3 Conclusions of WP2

- Screen printing of LaFeSi-based materials trialled, and binders developed that optimise impurity concentrations after binder removal.
- Several production methods investigated, including spherical particles and epoxy bonding
- An optimal method of part production was selected for deployment in WP5

## 3.3 WP3: Rare earth-free magnetocaloric materials for cooling and power generation

### Objectives

- To explore the relationship between structure and thermomagnetic hysteresis in RE-free materials
- To explore the potential for thermomagnetic power generation
- To produce films of FeRh-based alloys on conventional and piezoelectric substrates

### Summary of activities

The third material research strand has explored magnetocaloric systems that are **completely free of rare earths**, and which have not yet been produced in the forms such as thin plates required for their application as refrigerants. This strand employed not only bulk material preparation, but also deposition of compositionally-graded films, for **combinatorial analysis** of phase change properties, and theoretical modelling. **Our aim was to combine theory and combinatorial synthesis to understand how to tailor material properties, and to further new mechanisms for the magnetocaloric effect.** Furthermore, by extending our analysis to higher temperature ranges, this strand also explored materials for **high temperature power generation from waste heat.** This longer-term application of magnetocaloric materials uses heat instead of a magnetic field to bring about the phase change.

All objectives have been met: $(Mn,Fe)_2(P,Z)$ materials have been produced by high energy ball milling, and these have been passed to WP2. The effect of microstructure on the virgin effect in $(Mn,Fe)_2(P,Z)$ has been explored. Regarding power generation, (Mn,Co)B alloys have been further examined using experimental and theoretical tools. Thermodynamic data from La-Fe-Si and $(Mn,Fe)_2(P,Z)$-based materials have been gathered in order to test mean field models in WP4. Films of compositionally graded FeRhPt have been deposited and driven using a piezoelectric substrate. The latter results demonstrate a state-of-the-art level of control of the phase transition in a xtwo-dimensional space of electric and magnetic fields.

### 3.3.1 Structure-hysteresis relationship in RE-free magnetocaloric materials

The highlights presented in this section are arranged under two headings:

- Synthesis by novel routes of single phase Mn-Fe-P-Si
- Influence of microstructure on the virgin effect

*Synthesis by novel routes of single phase Mn-Fe-P-Si [CNRS Paris]*
Polycrystalline samples of $Mn_{1.3}Fe_{0.65}P_{0.5}Si_{0.5}$ were prepared by high-energy ball milling under Ar atmosphere as described in our associated publication.[22] From a relatively large quantity of nanocrystalline we synthesised samples of the same composition using different routes (powder annealing, classical sintering and SPS sintering). The powder synthesis route we used consisted of a two step annealing process: the polycrystalline sample was first annealed at 1373 K for 2 h in 200 hPa Ar atmosphere, and then at 1123 K for 20 h (the rate of temperature increase and decrease: 1.2 K/min). To produce the conventionally sintered sample, the fine powder was pressed into pellets (6 mm diameter) in Ar atmosphere. Then the pellets were sealed in quartz ampoules in 200 hPa Ar atmosphere and finally the same heat treatment was used as for the annealed powder samples. The third and fourth samples were prepared using Spark Plasma Sintering (SPS) from the annealed powder sample. The polycrystalline sample was heated up to 1223 K (using

[22] A. Bartok et al., Journal of Magnetism and Magnetic Materials **400,** 333-338 (2016).

temperature changing rate of 100 K/min) in Ar atmosphere under 50 and 80 MPa applied constant pressure and sintered for 30 min.

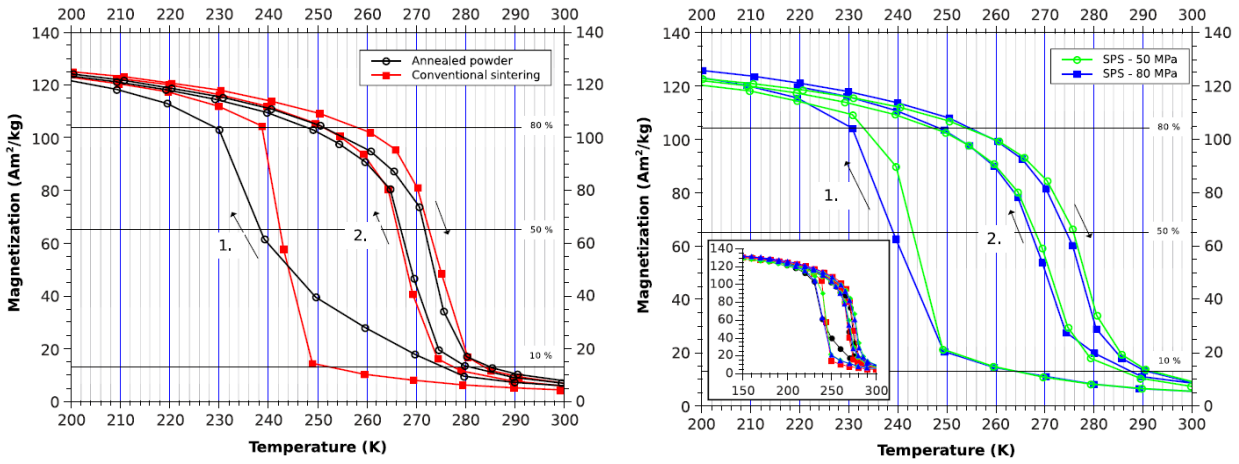


**Figure 3.11:** Temperature dependence of the magnetization, measured in 1 T applied field with increasing and decreasing temperature (2 cycles) on the as-prepared materials. Annealed powder sample (black hollow circles), sample prepared by conventional sintering (red full square), sample prepared by SPS under 50 MPa (green hollow circles) and 80 MPa (blue full square).

The temperature dependence of the isofield magnetization of the four samples is presented in Figure 3.11. Looking at the second and further cooling–heating cycles, all four samples show quite sharp paramagnetic to ferromagnetic transitions at around 270 K (here $T_C$ is estimated from the steepest point in the M(T) measured curves), with a thermal hysteresis of 5–7 K, and with a maximum magnetization of about 130 $Am^2/kg$ at 150 K, which is in a good agreement with the literature.[23] This is a further check of the absence of relevant differences of composition between the four samples.

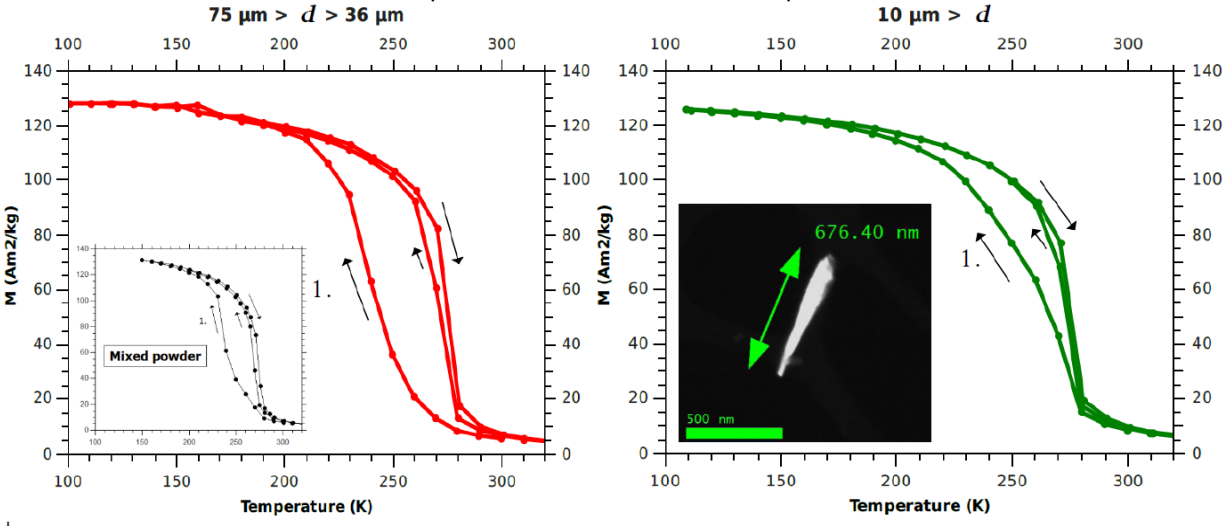


**Figure 3.12:** Temperature dependence of the magnetization, measured in 1 T applied field with increasing and decreasing temperature (2 cycles) on the as-prepared materials. Annealed powder sample with bigger grain size, (left) and fine powder (right).

The same isofield magnetization measurements have been carried out using a VSM in a temperature range 150 K < T < 320 K on annealed powder samples with different grain sizes. The temperature dependence of magnetization for two samples are presented in Figure 3.12. TEM images show that below 10 microns of grain sizes we are approaching the single crystal size limit. The powder sample with bigger grain size shows similar behaviour to that of the mixed powder. A reduced virgin-effect and thermal hysteresis can be observed in the case of the fine powder.

[23] N.H. Dung et al., Adv. Energy Mater., **1,** 6 (2011).

Further microstructure analysis has been made on the three bulk samples (prepared using conventional and SPS sintering methods). The grain structure has been visualized after chemical edging of the surface using a scanning electron microscope with Back Scattered Electron detector (BSE) at TU Darmstadt.

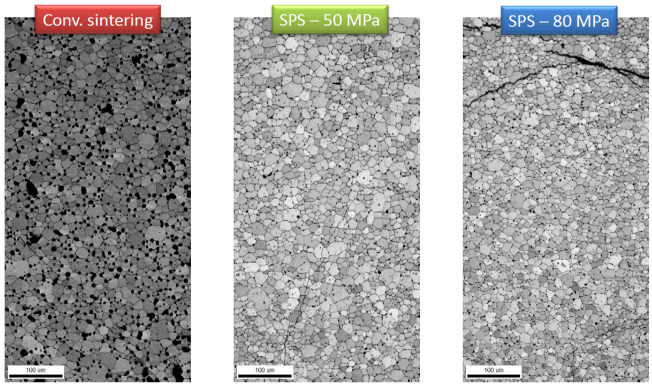


**Figure 3.13:** BSE images of the sample surfaces for bulk samples

Very high porosity (9%) can be observed for the sample prepared by conventional sintering compared with the SPS samples (1-2%). The average grain size is 17-18 microns using the conventional sintering method and SPS at 50 MPa. Using higher pressure during the SPS sintering decreases the average grain size considerably (12 microns).

The volume fractions and lattice parameters of the PM and FM phases of the mixed powder sample have been determined using Rietveld analysis of the XRD patterns. The temperature dependences of the FM fraction obtained from the refinement and the specific magnetic moment of the sample in a constant field measured by VSM are in good agreement, including the phase transition temperature and hysteresis.

It should be noted that the magnetic moment is proportional not only to the FM fraction, but also to the saturation magnetization vanishing at the Curie point. Comparison between the two methods (XRD and isofield magnetization measurements) is relevant because the extrapolation of phase fractions from magnetization data can be affected e.g. by a temperature dependence of the spontaneous magnetization.

*Influence of microstructure on the virgin effect [CNRS Paris and Imperial]*

The four samples described above were also examined by calorimetric methods and scanning Hall probe imaging. The DSC signals on first cooling are quite different; in the case of bulk samples they show a saw-tooth shape due to the presence of individual abrupt avalanche-like events. In this case we limit ourselves to detect the temperature interval where the VE takes place, $\Delta T_{DSC}$ by identifying the initial and final temperature of the first cooling transition as the points where the first cooling signal departs from the second cooling one. On examining the same DSC measurement configuration in the case of powder samples, a strong grain size effect can be observed. Below a critical average grain size (36 microns) the first cooling peak disappears. This observation corresponds to the isofield magnetization results.

Isothermal field-induced first (virgin effect) and further transitions have been imaged using a scanning Hall probe microscope (SHPM) on the conventionally sintered sample at Imperial. We followed the same protocol used to acquire isothermal magnetization curves with the PPMS (Figure 3.14). Virgin samples have been cooled to 250 K in zero magnetic field. Then images have been taken by increasing the field up to 4 T and decreasing it back to 0 T (Figure 3.14). Hall probe images allows us to visualize the jumps characterizing the first transition as sharp borderlines separating the FM regions bright in the images, from the dark PM ones (Figure 3.14, sequence 1). The smooth decrease of M, mainly due to magnetization rotation, is measured when reducing H to zero and is imaged as a gradual and uniform darkening of the sample (Figure 3.14, sequence 2). Optical microscope images of the as-prepared sample and of the same sample after the first transition show the formation of cracks that correspond approximately in shape and position to the boundaries between FM and PM regions visualized with the Hall probe.

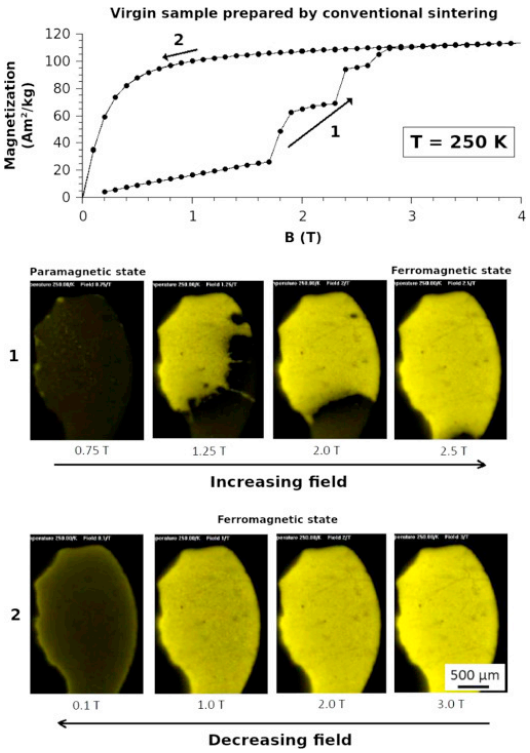


**Figure 3.14:** Isothermal magnetic measurements on the virgin sample prepared by conventional sintering at 250 K (top) and Hall probe imaging during measurement on the virgin sample prepared by conventional sintering at 250 K in increasing (center) and decreasing field (bottom). It is worth noting that the smooth darkening of the sample when the field decreases is entirely related to the rearrangement of M and that the first image (the darkest one) shows a sample still ferromagnetic in its remanent state.

Further magnetic measurements were carried out on a bulk Mn-Fe-P-Si sample prepared by conventional sintering from CNRS Paris. Stray field profiles and isothermal magnetization (at 275 K) loops have been recorded using a Hall-probe close to the sample surface (Figure 3.15 and Figure 3.16). When plotted along the y axis (line in the middle of the compacted sample), the high-field profiles look more flat, compared to the high-field profiles plotted along the x-axis (line from the middle to the board of the compacted sample). It is also clearly seen in the local loops in Figure 3.16, that all isotherms reach approximately the same value at 4 T, while the loops in Figure 3.15 are much more distributed.

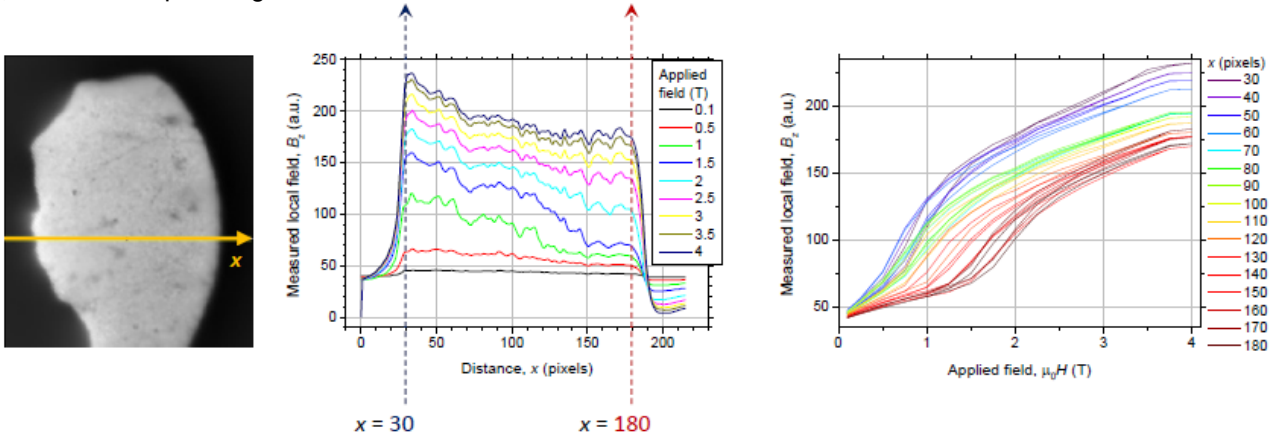


**Figure 3.15:** Field profiles along the indicated line x, extracted from Hall images at a set of applied field values. The image on the right shows static local loops at the x coordinate values indicated on the right of the plots. The plots are also extracted from Hall images.

An additional SEM/EDX study has been made to check whether the composition gradient is more pronounced along the x axis than along the y axis, but no compositional heterogeneity has been detected. We suggest that this observed gradient along the x axis is due to the gradient in the residual stress in the bulk sample. Calculations show[24] that in the case of conventional sintering the internal stress can be lower in the middle of the sample than in the board. As a consequence, due to the strong magneto-elastic coupling in the Mn-Fe-P-Si system, higher pressure can shift the *Tc* to lower temperature which is in a good agreement with our observations.

[24] Raul Valenzuela : Magnetic ceramics, Cambridge University Press, 1994.

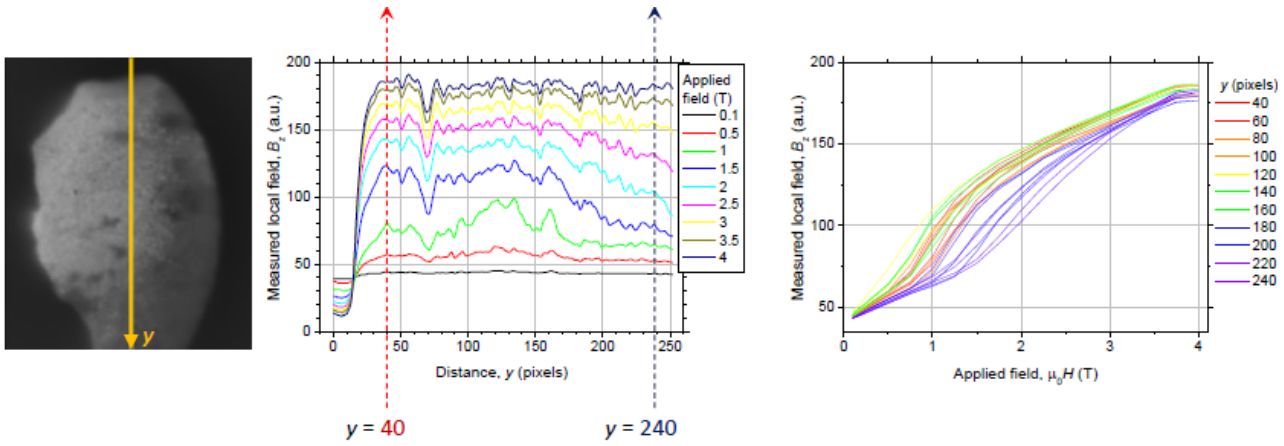


**Figure 3.16:** Field profiles along the indicated line y, extracted from Hall images at a set of applied field values. The image on the right shows static local loops at the y coordinate values indicated on the right of the plots. The plots are also extracted from Hall images.

### 3.3.2 Exploring the potential for magnetic power generation

Refractory borides are considered as good candidates for thermomagnetic energy conversion due to their high chemical stability and good magnetic properties. We have examined the tunability of the magnetic transition temperature of MnB by partial replacement of the transition metal with Fe and Co, respectively. In particular, we explored the magnetic, magnetocaloric and structural properties of the $Mn_{1-x}Co_xB$ and $Mn_{1-x}Fe_xB$ solid solutions. All produced samples crystallize in an orthorhombic Pnma structure with space group #62. In addition to the main phase, a small amount on $Mn_2B$ impurity phase (<3 wt.%) was found in many samples. The lattice parameters for all samples are shown in Figure 3.17 together with those calculated from first principles by Zsolt Gercsi (Imperial) within WP4.

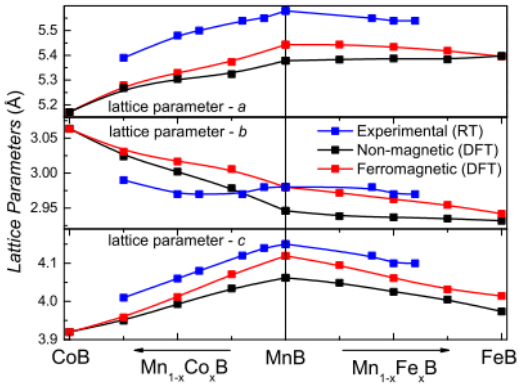


**Figure 3.17:** Evolution of lattice parameter with Co and Fe doping in MnB. The experimental results are compared to density functional theory (DFT) models of ferromagnetic and non-magnetic states.

The magnetic properties of all samples were determined including the spontaneous magnetization $M_s$, and Curie temperatures $T_C$. From Figure 3.18 (left and right) it is clear that substitution of Co on the Mn sites leads to a decrease in $M_s$ and $T_C$. Substituting Fe for Mn increases $T_C$ but does not yield a monotonic trend. This behaviour could be explained by theoretical calculations in WP4.

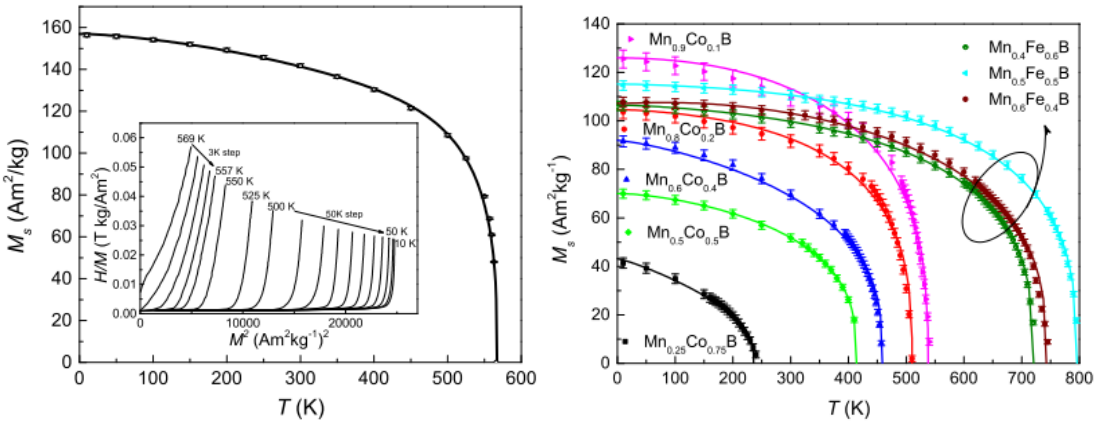


**Figure 3.18:** Left: Temperature dependence of the spontaneous magnetization of MnB. The points indicate the $M_s$ values obtained from Arrot-Belov plots. The inset shows the Arrot plot of the compound MnB derived from magnetic isotherms in a field changes of 0 T to 4 T at different temperatures. Right: Temperature dependence of the spontaneous magnetization of the system $Mn_{1-x}Co_xB$ and $Mn_{1-x}Fe_xB$ for different Co and Fe concentrations. Symbols indicate the$M_S$ values obtained from Arrot-Belov plots.

In summary, the pure MnB sample exhibits an orthorhombic structure with a spontaneous magnetization ($M_s$) of 156 $Am^2kg^{-1}$ and a sharp magnetic transition ($T_C$) of 567 K that yields a large magnetic field-induced entropy change of 7.5 $Jkg^{-1}$ $K^{-1}$ in a 0-2 T field change at this temperature. Both the substitution of Co and Fe elements for Mn were found to effectively modify $T_C$ accompanied by a lower magnetization ($M_s$) leading to a reduced magnetocaloric effect (MCE, see Figure 3.19). The sharp and significant change of $M_s(T)$, the very stable nature of these refractory borides and abundant availability makes some of these compositions suitable for thermomagnetic power generation applications in temperature range of 400-800 K.

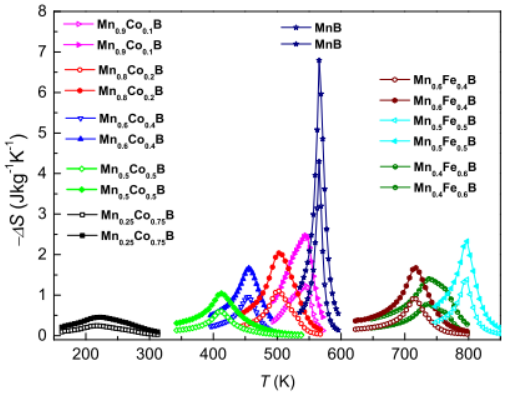


**Figure 3.19:** Magnetic field-induced entropy changes of the compounds MnB, $Mn_{1-x}Co_xB$ and $Mn_{1-x}Fe_xB$ in field changes of 1 T (empty symbol) and 2 T (full symbol) as derived from Maxwell relations.

### 3.3.3 Production of FeRh-based films on conventional and piezoelectric substrates

FeRh was selected as a model phase change material to explore magneto-elastic effects in RE-free magnetocaloric materials. Near the equiatomic composition, this material possesses a transition between low temperature antiferromagnetism (AF) and higher temperature ferromagnetism (F). Compositionally graded films were prepared by magnetron sputtering of composite targets consisting of a base of pure Fe (diameter = 75 mm) and superposed pieces of Rh foil of surface area 25x25mm$^2$. EDX analysis was used to estimate the spread in composition of as-deposited films. A 2D Fe:Rh composition map of a Ta 10nm/FeRh 250nm/Ta 1nm deposit on thermally oxidised Si made using 2 pieces of Rh is shown in Figure 3.20(a) and some sample magnetisation data are shown in Figure 3.20(b).

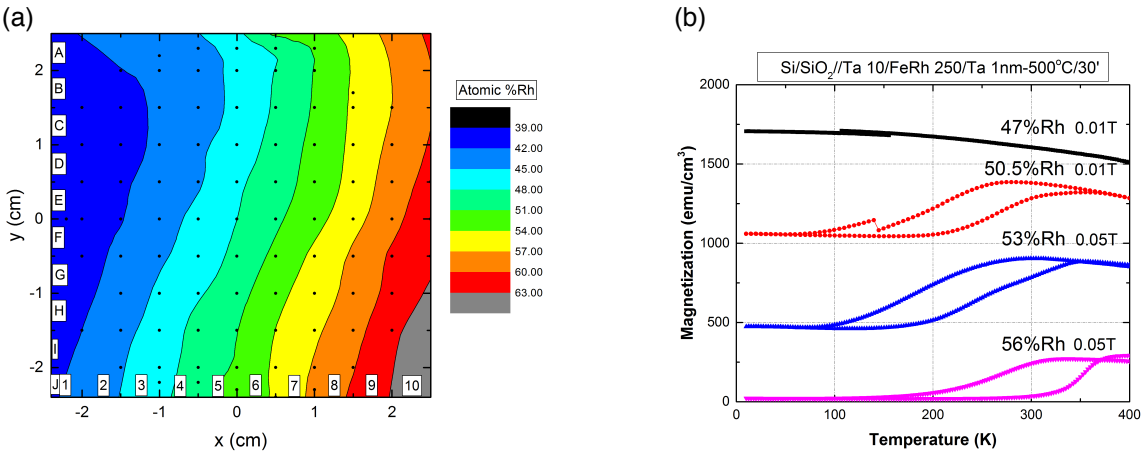


**Figure 3.20** (a) 2D composition map of an FeRh deposit as a function of position on the thermally oxidised Si substrate, for a composite target with 2 pieces of Rh superposed on a base Fe target; (b) - some sample M(T) curves of Ta /FeRh /Ta films. The latter are a function of composition and annealing conditions.

When Ta was replaced by Pt as the buffer and capping layers, diffusion of Pt into the FeRh film during the annealing process led to an increase in the transition temperature, a sharpening of the transition between and a reduction in the hysteresis (Figure 3.21(a)), in agreement with literature results.[25] Analysis of the XRD patterns of FeRhPt films revealed an almost linear decrease in the amount of bcc phase to 0 % as the

[25]J.S. Kouvel, J. App. Phys. **37,** 1257 (1966).

(Rh+Pt) content increases. An optical image of the compositionally graded FeRhPt film reveals a colour contrast between the Fe rich and Rh rich sides of the wafer (Figure 3.21(b)). Ellipsometry measurements across the sample reveal that a change in the reflectivity of the film occurs from one side of the transition to the other. This is in contrast to a previous report that the optical properties of antiferromagnetic and ferromagnetic FeRh are not different.[26] The position of the optical transition can be moved reversibly by heating and cooling the sample. A study of the temperature dependence of the optical transition, together with VSM measurements, has allowed us to construct the phase diagram of FeRhPt from a single deposition, which is in good qualitative agreement with that of the FeRh system.

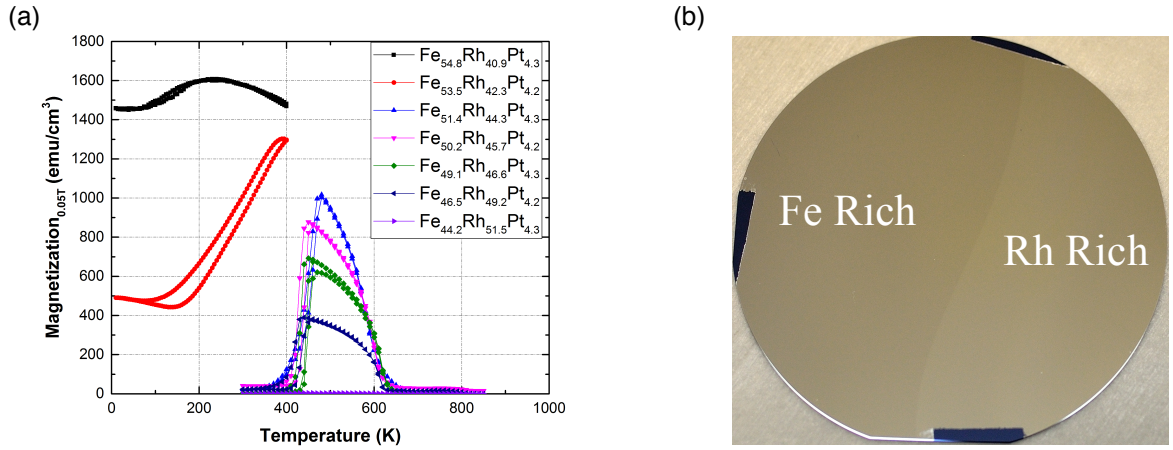


**Figure 3.21:** (a) - M(T) curves of samples from a compositionally graded Pt/FeRh/Pt film, following a post-deposition anneal which led to the diffusion of the Pt under and over layers into the FeRh layer. (b) An optical image of the compositionally graded FeRhPt film.

By replacing the Ta underlayer with Ni, we were able to reduce the transition temperature so that the transition that occurs upon cooling occurs below room temperature. As a result of the lower transition temperature, as we cross the phase diagram from the Fe rich to the Rh rich sides of the film we pass from ferromagnetism (F) to antiferromagnetism AF and back to F (i.e. we pass through the bump in the phase diagram). A bright AF band can be seen in optical photographs of the sample. Scanning Hall Probe imaging of the F-AF-F zone of the FeRhNi film was carried out at Imperial College London. The magnetic contrast observed due to the stray magnetic fields produced at interface between F and AF sections of the in-plane magnetised film prove that the optical transition coincides with the magnetic transition. Both interfaces were found to move upon cooling, with one of them returning to its starting position upon heating back to room temperature. The second interface did not reappear as the transition occurs above room temperature upon heating.

Both magnetic and structural phase changes exploited in magneto-caloric materials are strain sensitive. To study the influence of strain on phase transition characteristics (transition temperature, hysteresis), CNRS Grenoble proposed the deposition of magnetocaloric materials in film form onto piezo-electric (PMN-PT) substrates and to study the transition as a function of voltage applied to the substrate. This study involved the design, construction and testing of experimental set-ups to characterize and exploit the piezo-electric substrates, and then the preparation and study of piezo/magnetic layer composites. The influence of strain-induced changes in the AF-F transition in such samples was followed using 4-probe resistance measurements (Figure 3.22, left). Maximum values of $\Delta R/R$ of about 14% and 20 % were measured at 350 K for electric fields of 3 kV/cm (V = 80 V) and 18.7 kV/cm (V = 500V), respectively. Note that the strain achieved for a given electric field is temperature dependent, and that the actual strain achieved at 350 K is less than that measured at RT. Besides, the maximum voltage applied to the PMN-PT substrates was limited to 500 V when the substrate is stuck to a heating element, because application of higher voltages led to breakage of the substrates. The maximum strain-induced shift in the transition temperature was 20 K; which corresponds to 5 % of the absolute value (Figure 3.22, right).

Though beyond the time-frame of the DRREAM project, the influence of piezo-substrate induced strain on Pt and Ni doped films will now be studied. Modelling will also be performed to probe further the relation between strain and transition characteristics.

[26] L.-Y. Chen and D.W. Lynch, Phys. Rev. B **37,** 10503 (1988).

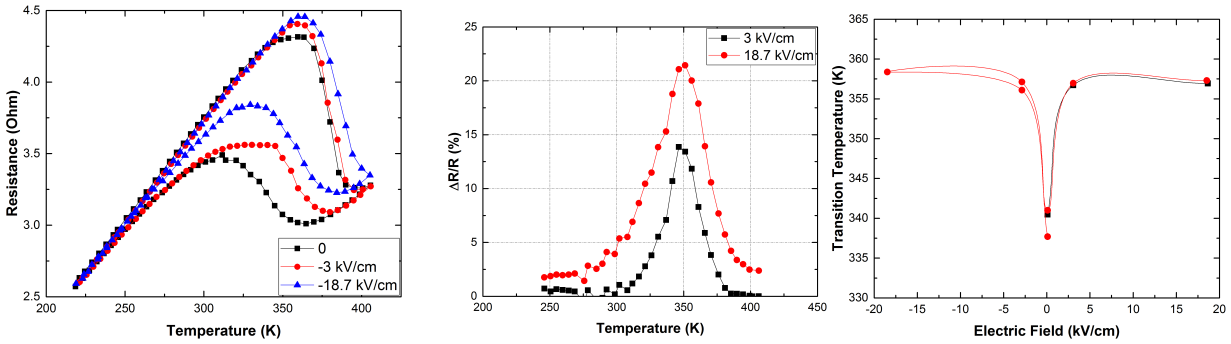


**Figure 3.22:** (Left): R(T) and (Middle) ΔR/R (T), measured on a 250 nm thick FeRh film deposited on an in-house polished PMN-PT (001) substrate. Measurements were made using a four-probe approach. (Right) The shift in AF-F transition temperature in FeRh films, estimated from R(T) measurements.

It should be mentioned that papers reporting on the influence of piezo-substrate induced strain on the AF-F transition in FeRh thin films were published during the timeframe of the DRREAM project. In Cherifi et al. (Nat. Mat, 2014), a shift in transition temperature of 25 K was achieved in 22 nm thick FeRh deposited on $BaTiO_3$ (001) substrates (applied voltage = 20 V; electric field = 0.4 kV/cm). In Lee, Ramesh et al. (Nat. Comm, 2015), an 8% change in resistivity was measured in 50 nm thick FeRh films deposited on PMN-PT (001). The changes in transition characteristics reported in these works are comparable to the values we achieved in the much thicker FeRh films (250 nm) that we studied. We can conclude that our films have state of the art properties and are thus suitable for further materials studies and eventually for integration into devices.

### 3.3.4 Conclusions of WP3

- Single phase MnFePSi materials produced by a variety of methods (not all shown here) and the correlation between grain size, preparation route and thermal hysteresis and the virgin effect was investigated
- Manganese borides investigated for high temperature, thermomagnetic power generation properties
- FeRhPt films produced on conventional and piezoelectric substrates

## 3.4 WP4: Theoretical modelling

### Objectives

- To model experimental results derived in WP1 and WP3
- To build *ab initio* models of RE-containing and RE-free magnetocaloric materials with transitions around and above room temperature

### Summary of activities

Theoretical modelling was a core part of our work. The dependence of magnetic properties in La-Fe-Si on transition metal substitution was examined. *Ab initio* work on Mn-antiperovskites has led to the prediction of an added value effect: large piezomagnetism in $Mn_3SnN$. A volume-dependent exchange model has been used successfully to describe the features of the magnetocaloric effect in first order LaFeMnSiH near its critical point. Lastly, the effect of material inhomogeneities on experimental Arrott plots has been examined. For reasons of space, not all of these activities are described below.

### 3.4.1 Ab initio modelling of magnetocaloric compounds

The highlights presented in this section are arranged under three headings:

- $Fe_2P$-based materials
- La-Fe-Si-based materials
- Mn-antiperovskites

*$Fe_2P$-based materials (Imperial College)*

A combined experimental-theoretical study of doped $Fe_2P$ compounds was carried out. The results described in brief here can now be found in published form.[27] Just as $La(Fe,Si)_{13}$ is the low-$T_C$, parent compound of the cobalt doped or hydrogenated room temperature magnetocaloric La-Fe-Si family, $Fe_2P$ is the low $T_C$ parent compound of the $(Mn,Fe)_2(P,Z)$ magnetocaloric material series. Upon substituting P for C or B, a very large increase in the ferromagnetic transition temperature is seen, from ~ 207 K in pure $Fe_2P$ to well above room temperature. In addition, the transition changes from first to second order. We set out to explain the large doping dependence of the Curie temperature found in this material family, to shed some light on the reasons why the parent compound is so suitable for magnetocaloric application and to pose theoretical avenues for further exploration.

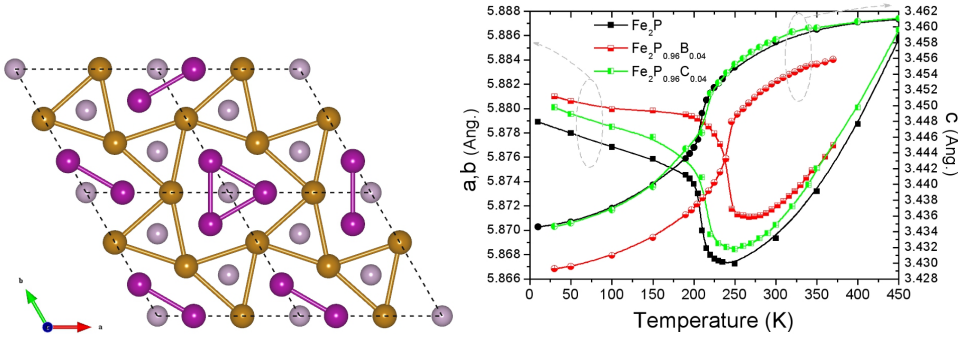


**Figure 3.23:** (Left) The crystal structure of $Fe_2P$, showing the two types of Fe site, FeI (blue) and FeII (orange). The P site is shown in grey. (Right) Temperature evolution of the lattice parameters of the parent $Fe_2P$ compound from neutron diffraction, together with that of the C- and B-doped samples. The strong magnetoelastic response is especially apparent around the magnetic ordering temperature (~215 K).

High resolution neutron diffraction was carried out on the HRPD instrument at ISIS, UK, and the structural parameters were used as starting inputs to a zero temperature model (VASP), where we use variations in structural parameters as a proxy for the effects of thermal expansion. From the neutron scattering data (Figure 3.23, right), we may see that there are counteracting changes in the basal plane and out-of-plane directions, across the magnetic ordering temperature. These can be shown to be due to changes in FeI-FeI, FeI-FeII and FeI-PI bond lengths (not shown).

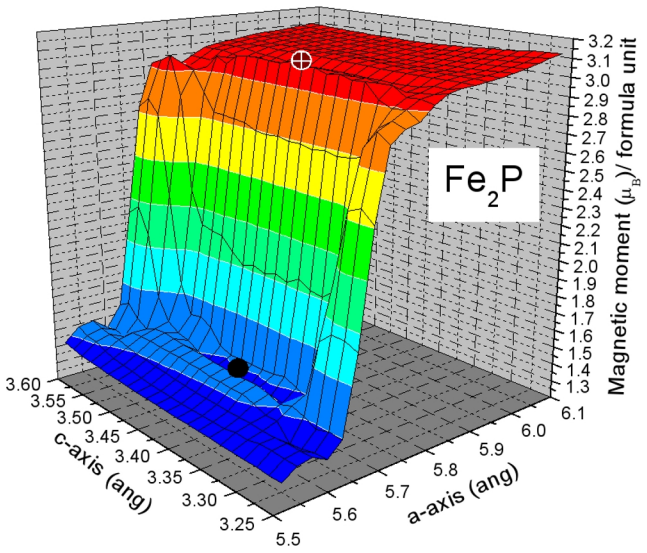


**Figure 3.24:** Total magnetic moment/formula unit as a function of lattice parameter of $Fe_2P$. The magnetic moment is strongly linked to the change in a-lattice parameter. The red and black dots indicate the high and low magnetization states (see text).

In the zero temperature calculations, the minimal, nine-atom basis cell (six Fe atoms and three P atoms) was used to evaluate the total energies and magnetic properties of the alloys. Using this simple model, the effect

[27] Z. Gercsi et al., Phys. Rev. B **88** 024417 (2013)

of doping was simulated by the replacement of a single phosphorous atom by another p-block element (Z) that represents an $x$ = 1/3 compositional change in the $Fe_2P_{1-x}Z_x$ formula. Although this approach is undoubtedly oversimplified in respect of exact compositions provided in the experimental section, we believe it is still a suitable model to capture the relevant changes in the electronic structure caused by the dopant elements. In order to be consistent with the experimental results, we only considered changes along the *a* and *c* axis by the individual expansion and compression of the *a*- and *c*-lattice parameters, without allowing any relaxation of the strained structure. In practice, we varied the lattice parameters using a step size of ±0.5%, calculating the self-consistent electronic structures at each step.

The calculated variation of total magnetization in the FM state with lattice parameters is plotted in Figure 3.24. A small change in the lattice can have a very strong effect on the magnetic properties. The lattice expansion within the basal plane causes the total magnetic moment/formula unit to increase abruptly from ~ 1.3 $\mu$B to 3.1 $\mu$B around a critical value of $a \approx 5.7$ Å, and stays practically constant above it. The magnetisation varies very little with *c*, reflecting the greater importance of the atomic distances within the basal plane, where the atoms are packed more densely. The calculations reveal the unusual duality of the magnetic structure of $Fe_2P$ in which there is a large magnetic moment of M(FeII ) = 2.16 $\mu$B on the 3*g* site together that coexists with a significantly smaller, M(FeI) = 0.85 $\mu$B, moment on the 3*f* crystallographic site. These findings are in full agreement with previous studies. We find a redistribution (delocalization) of the magnetization from the 3*f* site along the FeI-PII chains in the *c*-axis direction occurs, implying its strong influence on bonding (also suggested by Dung et al.[23])

Our DFT analysis therefore finds that the magnetization is highly sensitive to the change in lattice dimensions, therefore both compositional inhomogeneities and internal strains as set by the preparation conditions can significantly alter the observed magnetic properties of the material. For applications (such as magnetic refrigeration), where the transition temperature needs to be set by the material to a high accuracy, elements such as Si and As are favourable but process control will be crucial. We have also successfully described the preferred site occupancy of particular dopants. Further details are given in our published manuscript.[27]

*La-Fe-Si-based materials (Imperial College)*
A model of the effect of H, B, C, and N interstitials on the magnetism of La-Fe-Si materials was constructed in collaboration with Asaja Fujita (Tohoku University, Japan). The model used was that of a parent $LaSiFe_{12}$ alloy. We found that this material has a shallow, double-well free energy function that is the basis of first order itinerant electron metamagnetism. On increasing the dopant concentration, the resulting lattice expansion causes an initial increase in magnetisation for all interstitials that is only maintained at higher levels of doping in the case of hydrogen. Strong *p-d* band hybridisation occurs at high B,C and N concentrations. We thus found that the electronic effects of hydrogen doping are much less pronounced than those of other interstitials, and result in the double-well structure of the free energy function being least sensitive to the amount of hydrogen. This microscopic picture accounts for the change in the metamagnetic transition from first order to second order on doping with B,C, and N interstitials, as observed experimentally, and complements aspects of a picture developed by Kuz'min and Richter for the undoped material.[28]

Consequently, hydrogen provides perhaps the only chemical pressure on the lattice that avoids significant alterations to the electronic structure of $LaSiFe_{12}$. In the case of the other dopants (B, C, N) broad bands originating from their p-states appear at energy levels, where the 3d states of Fe are also present. The formation of these hybrid *p–d* bands results in the disappearance of the peak and valley structures in the electronic density of states around the Fermi energy, thereby reshaping the shallow free energy landscape and ultimately destroying the first order itinerant electron magnetism of $LaSiFe_{12}$.[29]

In further work, evidence for antiferromagnetic coupling between Fe and Mn or Cr was found in the case of $LaFe_{11.5}TM_{0.5}Si$. Full results are given in the relevant publications.[30]

*Mn-based antiperovskites (Imperial College)*
In the last 7 years, metallic perovskites, first examined in the 1970s, have become the focus of renewed investigation. The magnetocaloric effect of carbides such as $Mn_3GaC$ has been examined in the neighbourhood of a metamagnetic transition between an antiferromagnetic groundstate and an intermediate

[28] M. D. Kuz'min and M. Richter, Phys. Rev. B **76,** 092401 (2007).
[29] Z. Gercsi, N. Fuller, A. Fujita and K.G. Sandeman arXiv:1407.7975 (2014).
[30] Z. Gercsi, Europhysics Letters **110,** 47006 (2015).

temperature ferromagnetic state at around 160 K. Meanwhile, nitrides such as $Mn_3(Cu,Ge)N$ have enjoyed a revival of interest because of the discovery of large, negative thermal expansion (NTE) associated with a first order Néel transition in $Mn_3CuN$ which may be broadened by the (Cu,Ge) substitution.[31]

We completed the VASP calculations of the piezomagnetic effect (PME) for a set of 9 cubic metallic Mn-antiperovskites $Mn_3AN$ (A = Rh, Pd, Ag, Co, Ni, Zn, Ga, In, Sn)[32] where Takenaka et al. measured negative thermal expansion[33] (NTE). Firstly, we were able to identify a correlation between the size of PME and the mean valence band energy of atom A, thereby accounting for the magnitude of the induced net moment $M_{net}$ based on features of the ground state electronic structure, as shown by Figure 3.25.

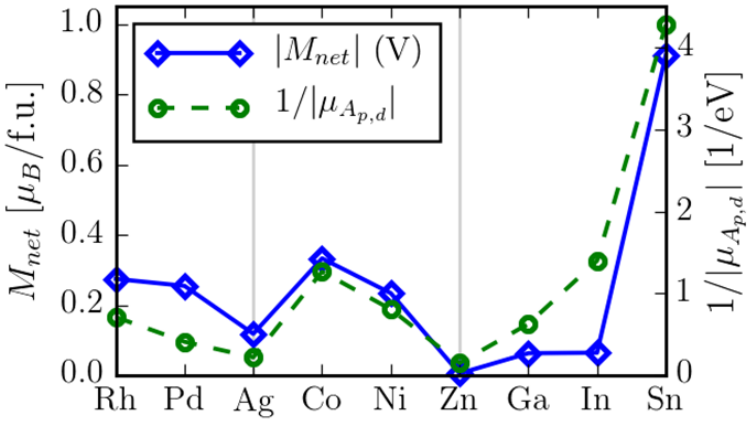


**Figure 3.25:** Net magnetic moment induced by biaxial strain of 1% and the inverse of the mean energy of the valence p- or d-states of atom A compared across the full set of cubic $Mn_3AN$.

Secondly, we introduced a piezomagnetic susceptibility $\chi_P$ which quantifies the response of the frustrated antiferromagnetic structure to applied strain and compared this quantity to the NTE data (measured as spontaneous volume change $\omega_s$ at the Néel transition) across the set of 9 materials. Figure 3.26 shows that the PME calculated at zero temperature and the NTE measured at Néel temperature are inversely proportional. This correlation may be used as a tool in the theory-led design of non-stoichiometric Mn-antiperovskites with large NTE.

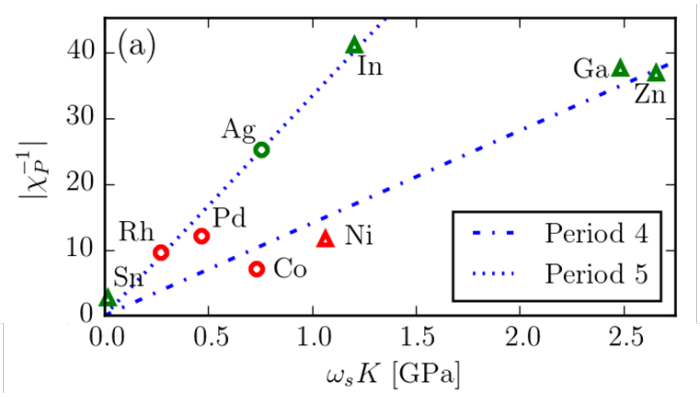


**Figure 3.26:** The inverse of piezomagnetic susceptibility (a measure of PME) as a function of the spontaneous volume change at the Néel temperature (multiplied by bulk modulus K) for 9 $Mn_3AN$ compounds.

Furthermore, a large spontaneous volume change is an indicator of a large entropy change at the antiferromagnetic to paramagnetic phase transition so the same tool can be used to identify Mn-antiperovskites with mixed composition suitable for solid state cooling applications.

[31] K. Takenaka and H. Takagi, Appl. Phys. Lett. **87,** 261902 (2005).
[32] J. Zemen, Z. Gercsi, K. G. Sandeman , arXiv:1512.03470 (2015)
[33] K. Takenaka, Sci. Technol. Adv. Mater. **15,** 015009 (2014)

Thirdly, we calculated the dependence of $T_N$ on applied biaxial strain using finite-temperature *ab initio* (DLM-KKR) methods in collaboration with Prof J. Staunton.[34] Figure 3.27 shows that $Mn_3GaN$ has the strongest dependence of $T_N$ on strain which makes it a suitable candidate for hosting a large elastocaloric effect.

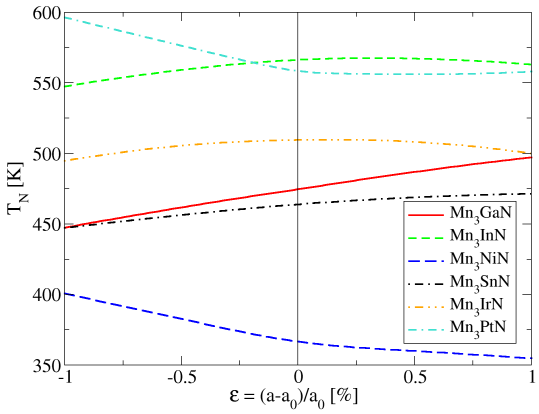


**Figure 3.27:** Néel temperature as a function of biaxial strain calculated using KKR-DLM methods.

### 3.4.2 Thermodynamic modelling of La-Fe-Si materials

*INRIM contribution*

Modeling the measured behaviour of these systems is of primary importance for the further optimization of the material. Our thermodynamic modelling of these materials takes into account magnetoelastic effects by introducing an explicit dependence of the exchange interaction on the specific volume, as proposed by Bean and Rodbell[35]. The model is based on the fact that the exchange interaction may depend on the distance between magnetic atoms. As volume change is reflected by an overall change in the interatomic distances, Bean and Rodbell described this effect by introducing a Curie temperature depending on the lattice reduced volume $\omega = (v - v_0)/v_0$, v, $v_0$ being the deformed and equilibrium specific lattice volumes, respectively, as $T_c = T_0 (1 + \beta \omega)$, with $\beta$ being a dimensionless coefficient describing the magnetoelastic coupling and $T_0$ the Curie temperature at $\beta = 0$.

*Materials.* We have taken the experimental data concerning the series of Mn substituted $La(Fe\text{-}Mn\text{-}Si)_{13}\text{-}H_{1.65}$ samples. In hydrogenated $LaFe_xMn_ySi_z$ compounds (with x + y + z = 13) the transition temperature can be finely tuned by Mn substitution[36]. The material shows, with Mn increasing from y = 0.06 to y = 0.46, a transition temperature changing from 339 K to 270 K, an entropy change (at 1.5 T field) which goes from 18.7 $Jkg^{-1}K^{-1}$ to 10.2 $Jkg^{-1}K^{-1}$, and a temperature hysteresis going from 1.5 K to 0 K. The specific heat measured by Peltier calorimetry in magnetic field is shown in Figure 3.28.

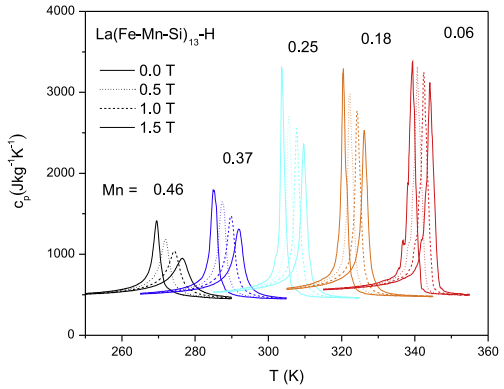


**Figure 3.28:** Specific heat capacity of hydrogenated $La(Fe\text{-}Mn\text{-}Si)_{13}$ with different Mn content. Measurements upon heating at different magnetic fields.

[34] J. B. Staunton et al., Phys. Rev. B **87,** 060404(R) (2013).
[35] M. Piazzi, C. Bennati, C. Curcio, M. Kuepferling and V. Basso, J. Magn. Magn. Mater. 400, 349 (2016)
[36] V. Basso, M. Kuepferling, C. Curcio, C. Bennati, A. Barzca, M. Katter, M. Bratko, E. Lovell, J. Turcaud, and L. F. Cohen, J. Appl. Phys. **118** 053907 (2015).

| Fe | Mn | Si | $T_0$ (K) | $\mu_0 H_0$ (T) | $\eta$ |
|---|---|---|---|---|---|
| 11.22 | 0.46 | 1.32 | 272 | 405 | 1.0 |
| 11.33 | 0.37 | 1.30 | 286 | 426 | 1.1 |
| 11.47 | 0.25 | 1.28 | 305 | 455 | 1.15 |
| 11.60 | 0.18 | 1.22 | 320.5 | 478 | 1.2 |
| 11.76 | 0.06 | 1.18 | 339 | 505 | 1.2 |

**Table 3.1:** Parameters used to model the entropy change behavior of $La(Fe_xMn_ySi_z)13–H_{1.65}$ samples with compositions x (Fe), y (Mn), z (Si).

To compare the model with experimental data have used the magnetic field induced entropy change. In the model we have fixed J = S = 1/2 and the remaining free parameters η, ζ, $T_0$ and n are determined according to the procedure described in [37]. As a result we have found a good agreement with experiments with the parameters of Table 3.1 and the same $nk_B$ = 170 J $kg^{-1}K^{-1}$ and ζ = 0.25 for all the samples.

The values found shows that η vary approximately linearly with $T_0$. By making a linear fit of the values reported in the above table versus the corresponding $T_0$ values we find a linear coefficient of $3.7x10^{-3}$ $K^{-1}$. The latter can be used to determine the value of β. By taking a literature value for the compressibility $\kappa_T = 8.6 \times 10^{-12}$ $Pa^{-1}$ we find $\beta \simeq 15$ for all the samples, independently on the Mn content. This value appears reasonable in comparison with other estimates made on different magnetocaloric materials. At the same time as $\zeta = \alpha_p \beta T_0$, we have another relation linking this time β and ζ. We have therefore an alternative independent route to check the feasibility of the chosen value of ζ, i.e. $\zeta \simeq 0.25$. If we use $\alpha_p \simeq 5 \times 10^{-5}$ $K^{-1}$, the typical value of the thermal expansion coefficient for iron alloys (that in the model should be an expansion due to the lattice only) we end up with ζ values ranging between 0.20 and 0.25, depending on the transition temperature. Since we do not have a very precise method to fit with accuracy ζ from the experimental data, the fact that the value fixed at the beginning, i.e. $\zeta \simeq 0.25$, is within the calculated range is quite satisfactory. This result provides global coherence of the whole modeling approach and shows that the main role of Mn is reflected exclusively in a decrease of the strength of the exchange interaction, while the value of the coefficient β, responsible for the coupling between volume and exchange energy, is independent on the Mn content and it appears to be an intrinsic property of the $La(Fe,Si)_{13}$ structure.

### 3.4.3 Conclusions of WP4

- Ab initio models of several familes of magnetocaloric materials (shown here) and thermomagnetic materials (not shown for space reasons)
- Prediction of large piezomagnetism in Mn antiperovskites
- Agreement between thermodynamic models and experimental data on La-Fe-Si alloys
- Influence of inhomogeneities on Arrott plots (not shown for reasons of space)

[37] M. Piazzi, C. Bennati, C. Curcio, M. Kuepferling and V. Basso, J. Magn. Magn. Mater. 400, 349 (2016)

## 3.5 WP5: Impact on rare earth use

### Objectives

- Bespoke testing of magnetocaloric parts in regenerator structures
- Analysis of mechanical and chemical integrity including corrosion testing
- Final life cycle comparison of theoretical magnetic refrigerator and conventional domestic refrigerator

### Summary of activities

From WP2, an optimal production route was chosen. Plates of Co-doped LaFeSiCo and Mn/H doped were produced. This was the first time, to our knowledge, that LaFeSiMnH had been successfully integrated into single material regenerator parts and further integrated to form a multi-material cascade. Prior work is based on powder bed morphologies - which are inherently less efficient because of enhanced pressure drops.

With the successful development of high-performance LaFeSiMnH regenerators (with enhanced magnetocaloric effect), the projected magnetic field of the system can be lowered - a key element to achieving the overall rare-earth reduction targets.

Regarding non-magnetocaloric properties, the Young's Modulus, breaking strength and hardness of the LaFeSi system were measured. The corrosion properties of plastic bonded materials were also examined, as were the use of improved inhibitors, and nano-glass coatings. This activity doubled the durability of the LaFeSiCo material in real life use cases.

The chosen production route in WP2 reduces material wastage by 33%. However, projected rare earth usage in the permanent magnets falls by 75% Based on the LCA analysis, the total rare earth usage has fallen by 73%.

### 3.5.1 Testing of magnetocaloric parts

Parts produced using three different techniques were examined: 2 subtractive and 1 additive method. Mechanically, all three approaches yielded shaped parts. The level of prevision of each method is shown in Figure 3.29. In terms of precision, the subtractive methods are superior to the additive approaches. Magnetocalorically, the additive approach did not yield magnetocalorically active shaped parts, but both the subtractive methods yield an MCE that was comparable to the original bulk material. This is demonstrated in Figure 3.30.

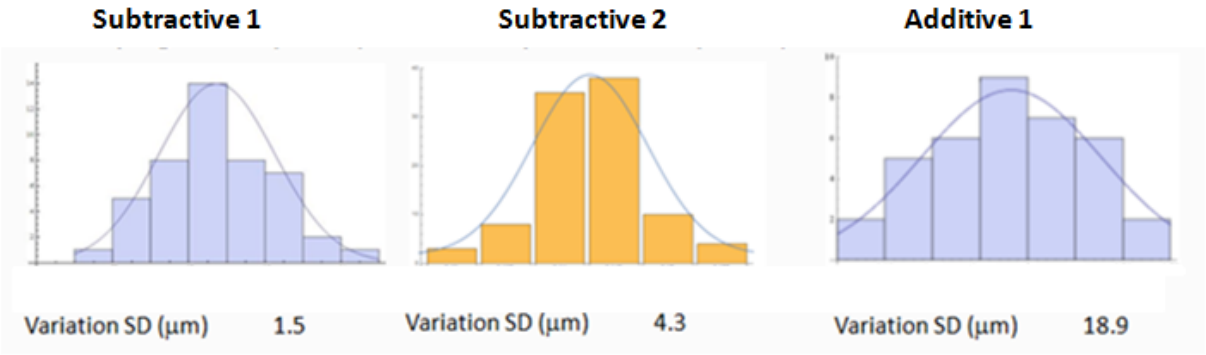


**Figure 3.29:** Comparison of processing precision of three different production routes (Camf)

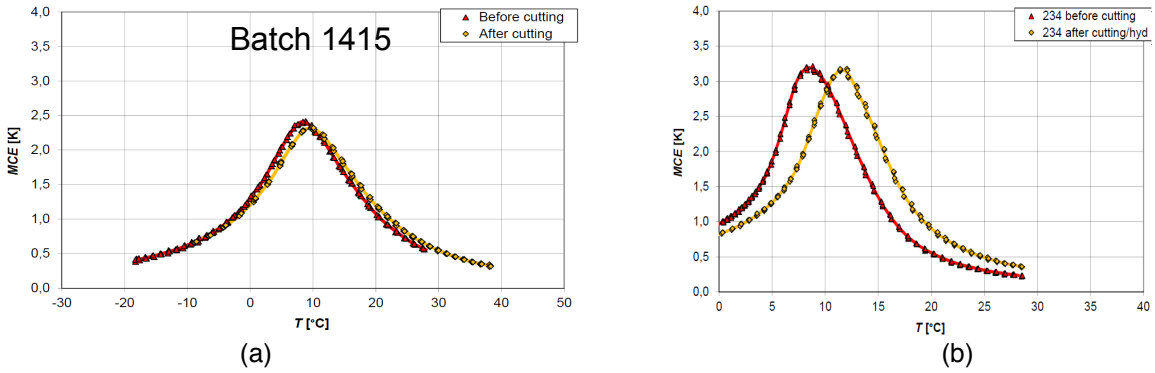


**Figure 3.30:** Comparison of magnetocaloric effect before and after subtractive processing (a): LaFeSiCo, (b) LaFeSiMnH (VAC)

In both cases the size of the magnetocaloric effect is preserved before and after processing; however in the LaFeSiMnH a shift in Curie temperature was observed. Both the LaFeSiCo and LaFeSiMnH shaped parts were assembled into regenerator components. The interesting result is that the LaFeSiMnH parts - rendered significantly more brittle than the LaFeSiCo as a result of the hydrogenation process - were nevertheless sufficiently mechanically stable to enable regenerator assembly, survive magnetic field cycling to yield a high performance cascaded regenerator structure. This is the first time (to the author's knowledge) that high-performance shaped parts (rather than less efficient powder structures) of LaFeSiMnH have been successfully fabricated. Some regenerator data is presented in Figure 3.31.

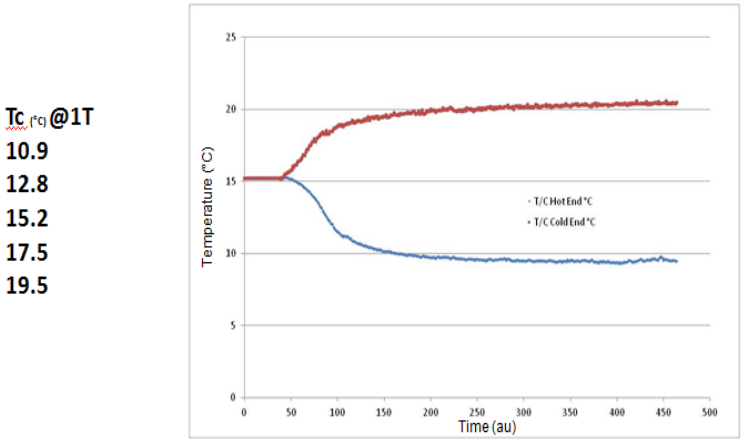


**Figure 3.31:** Temperature profile across a five material LaFeSiMnH cascade regenerator made of shaped parts.(Camf)

Furthermore, pressure flow testing demonstrated that the regenerator components possessed a linear pressure-flow relationship which is consistent with laminar theory (Figure 3.32).

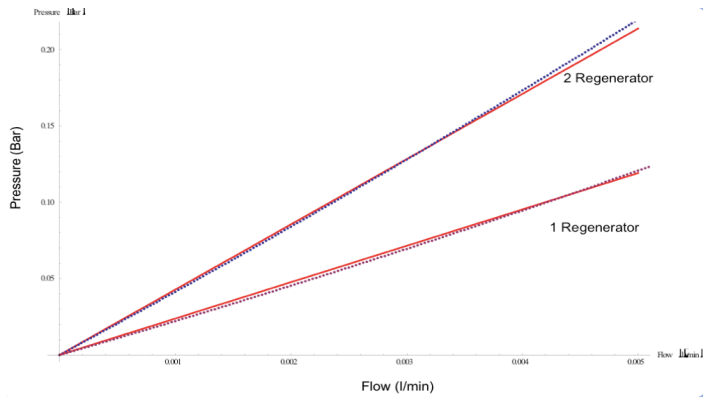


**Figure 3.32:** Red-lines (measured values), Dotted lines (theoretical values) (Camf)

### 3.5.2 Analysis of mechanical and chemical integrity including corrosion testing

*Mechanical: Breaking strength of LaFeSiCo*
Flexural strength was examined using 4-point bending following ASTM C1161 with geometry 25 mm x 4 mm x 3 mm. Tests were conducted on LaFeSiCo samples with $T_C$ 5°C, 40°C, 50°C 60°C. In this destructive test method a mechanical load is applied to the specimen until fracture occurs.

The tests were performed on 25 samples at room temperature and the results are summarised in Table 3.2.

| Curie Temperature | MCE in 1T | Range of breaking stresses | Characteristic break strength | Weibull shape parameter | Coefficient of determination |
|---|---|---|---|---|---|
| $T_c$ [°C] | ΔT [K] | σ [MPa] | $\sigma_0$ [MPa] | m | $R^2$ |
| **5** | 1.68 | 119 - 190 | 173.3 | 10 | 0.98 |
| **40** | 1.54 | 124 - 182 | 157.4 | 11 | 0.89 |
| **50** | 1.50 | 133 - 170 | 154.7 | 17 | 0.92 |
| **60** | 1.43 | 121 - 162 | 152.8 | 16 | 0.97 |

**Table 3.2:** Breaking strength of LaFeSiCo samples (TUD)

*Mechanical: Young's Modulus*
Resonance frequency damping analysis (RFDA) was used to study the Young's modulus, *E*, as a function of temperature. This method is a non-destructive means of measuring the elastic properties of a specimen. A mechanical impulse causes the specimen to vibrate. Due to the correlation of the elastic properties to the mechanical resonance frequencies, the mechanical properties can be determined by analysing the frequency pattern.

VAC supplied dedicated material for this test. The optimal geometry for and flexural testing are rods: 3 x 4 x 25 mm. VAC supplied about 50 rods of La-Fe-Co-Si of each of the following Curie temperatures: 5, 40, 50, and 60°C. A reduction in the Young's modulus is found near the Curie temperature.

*Mechanical: Indentation Testing*
Indentation testing was used to examine hardness, the resistance to permanent deformation. In addition, indentation testing provides another measurement of elastic modulus. The results are shown in Figure 3.33. Elastic modulus from indentation testing was found to be 130±5 GPa. The hardness was found to be 8±0.5 GPa.

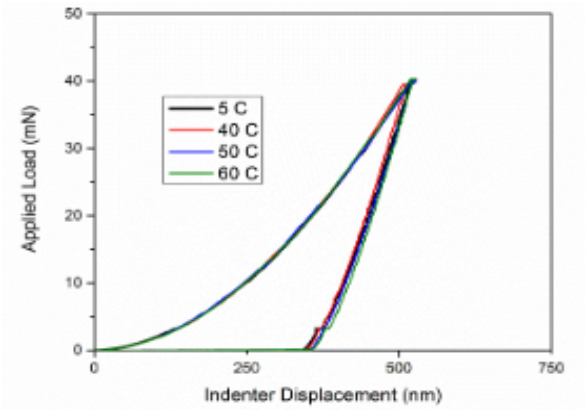


**Figure 3.33:** Indentation testing: applied load versus indenter displacement for La-Fe-Si (TUD)

*Corrosion Testing*

A range of coatings and inhibiters were examined, and the lifetime of the parts was increased by 100%. Figure 3.34 illustrates a comparison of corrosion rates between polymer bonded and uncoated solid parts using standard (non-inhibited) fluids and gases.

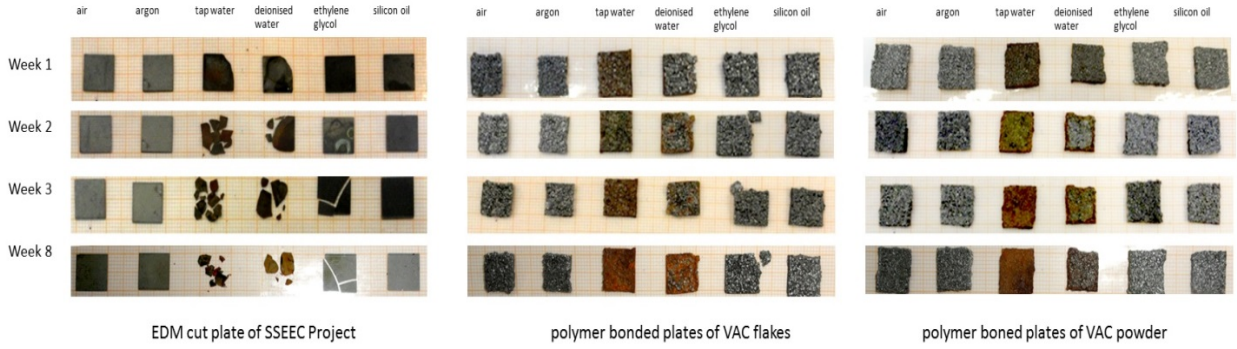


**Figure 3.34:** Corrosion comparison of solid and bonded LaFeSiCo

### 3.5.3 Life cycle comparison of theoretical magnetic refrigerator with conventional domestic refrigerator: innovations over the length of the project

The development of physical prototypes was not allowed under this call. Although the initial life cycle analysis (LCA) was based on the state of the art prototype at the start of the project, the final LCA had to be developed on the basis of a virtual prototype - how a system would look if it incorporated the key advances developed within the project.

The advances developed within the project and incorporated into the virtual prototype include:

- Use of shaped LaFeSiMnH regenerators, which deliver a 50% improvement in cooling performance over the baseline material, without impacting efficiency (through the shaping achieved compared to the baseline design). See Figure 3.35.
- To maintain the same baseline cooling power, and utilising the enhanced magnetocaloric effect materials, a lower magnetic field was incorporated into the virtual prototype.
- The impact on performance of improved shaping (and shaping precision) of the materials was also incorporated into the LCA.

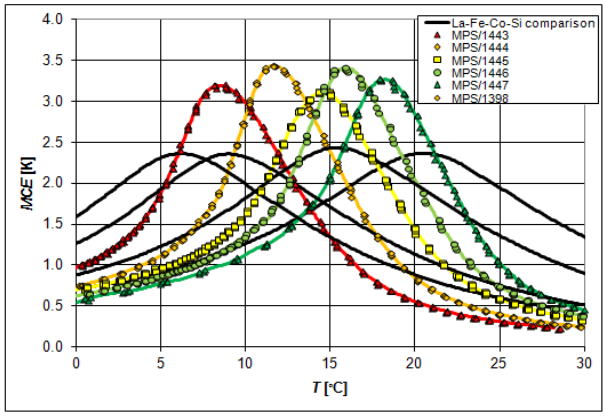


**Figure 3.35:** Comparison of magnetocaloric effect of baseline material La-Fe-Si-Co (black lines) with new shaped materials of La-Fe-Mn-Si-H (coloured lines) developed over the life of the project. (VAC)

*Overall Environmental Benefits*

A comparison of the two life cycle analysis (LCA) studies (at the beginning and at the end of project) shows that the innovations introduced during the project reduced the impact of the considered life cycle of almost 13%, in terms of Ecopoints (Figure 3.36), and more than 12%, in terms of GWP.

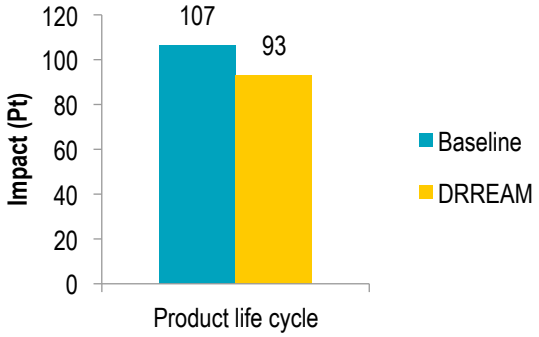


**Figure 3.36:** Comparison of the environmental impact of the life cycle of the two prototypes. (Indesit)

*Impact on Rare-earth Usage*

From the LCA, the impact upon rare-earth usage, the following results can be summarised:

- The best subtractive method reduces wastage by 33% (just short of a project target of 40%), and the additive method demonstrably reduced wastage by 93% (well in excess of the 40% target), albeit without simultaneously achieving optimally shaped, magnetocalorically active parts.
- Rare earth usage in the permanent magnets has fallen by 75%, significantly beating an original 25% target.
- Based on the LCA, the total rare earth usage has fallen by 73% - significantly beating a 55% target set at the start of the project.

### 3.5.4 Conclusions of WP5

WP5 has achieved all of its goals:

- Demonstrated the operation of LaFeSiMnH shaped regenerators, which deliver a 50% improvement in cooling performance over the baseline material (through an enhanced magnetocaloric effect), without impacting efficiency (this latter outcome as a result of superior shaping compared to the baseline design).
- Rare earth usage in the permanent magnets have fallen by 75%
- Based on the LCA analysis, the total rare earth usage has fallen by 73%

**As a result of the above, we believe that the *DRREAM* project has contributed to a major development: the reduction of magnetic field required in a domestic cooling engine.**

# 4. Potential impact and main dissemination activities

## 4.1 Potential impact

We have aimed to develop knowledge of phase transition magnetic materials and their manufacture to bring about an integrated response to the need to decrease the rare earth footprint of magnetic cooling. Our assessment of impact on RE use requires this fully integrated approach and has been fed back to all steps of our work: theoretical modelling, bulk fabrication, film growth and manufacture. We have leveraged our material innovations to explore the prospects for novel technologies such as thermomagnetic power generation and so expect to achieve several impacts, which are now listed.

### 4.1.1 Availability of high-performance materials

*Magnetic cooling*

Our work on LaFeSi-based and RE-free magnetocaloric materials will provide not only a set of compositions but also manufacturing routes for these complex systems. Today, approximately one third of the energy consumed in EC countries is destined to comfort in buildings (heating, air cooling and air exchange). Significant $CO_2$ savings can be made by adopting low energy consumption technologies in this sector. A recent study predicted that HFCs could account for between 28 and 45% ($CO_2$-equivalent basis) of projected global $CO_2$ emissions by 2050[38]. The replacement of these with solid, magnetic refrigerants will therefore play a role in achieving greenhouse gas target in the medium term.

*Further innovative applications*

While our end use focus is primarily on magnetic cooling, the potential impact of our magnetocaloric materials is even wider and has been explored in relation to thermomagnetic power generation as well. Energy harvesting using photovoltaic or thermoelectric materials is already receiving significant attention. We believe that it will be very attractive to leverage our advances in the fabrication and manufacture of low rare earth content magnetic phase change materials to provide power from thermal gradients.

Furthermore, the thin films samples that have be developed in this project have potential applications in micro-systems. By coupling a magnetic phase-change material to a piezoelectric material, we may deform the former in a controlled fashion. However, such a couple could also be used to generate electricity in the piezo-material by a temperature or field induced *deformation* of the magnetic material. Use of a magnetic phase-change material in this capacity could allow the development of multi-modal (T and H) energy harvesters. **Thus the study of magnetic phase-change materials in film form in this project could have direct impact on the future development of low-power energy-harvesting micro-systems.**

Lastly, our theoretial work has predicted the existence of giant piezomagnetic effects in certain Mn-based antiperovskites. The ability to control and switch magnetism via strain could have a variety of uses in spintronics.

### 4.1.2 Availability of magnetic materials with reduced reliance on critical raw materials (CRMs)

As detailed in section 2, clean energy technologies and efficient energy use technologies are both expected to require an increasing fraction of the world's critical materials supply in the coming years[39]. **The project's ultimate accomplishment of a 74% reduction in total rare earth usage (predominantly Nd and La) in magnetic cooling technology,** will hopefully position magnetic cooling for more widespread adoption,

As outlined earlier, consumer pressure is also driving the refrigeration sector to examine more efficient technologies. In the last 15 years, the most efficient cooling technology has always become that which consumers favoured. Figure 4.37 shows this historical trend, and the market projections for the A+++ based on market analysis by three of Europe's leading domestic appliance manufacturers. The refrigeration market is clearly a very dynamic one, with the proportion of sales of A+, A++ and A+++ efficiency devices (shown in different colours in Figure 4.37) changing significantly year on year.

[38] G.J.M. Velders et al., Proc. Natl. Acad. Sci. USA. **106** 10949 (2009).
[39] O. Gutfleisch et al., Adv. Mat. **23** 821-842 (2011).

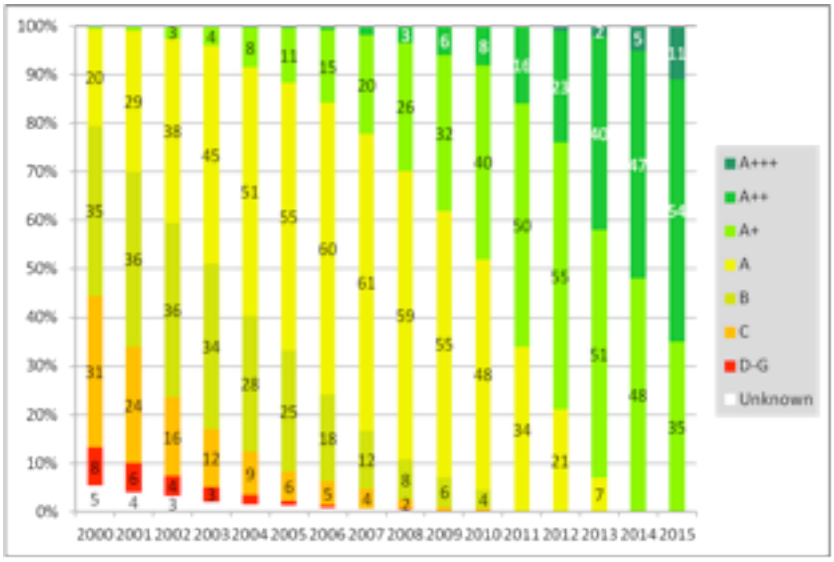


**Figure 4.37:** Consumers are rapidly changing towards increasingly energy-efficient refrigeration devices. Source: Historical Data GFK; projections based on market data from Camfridge's refrigeration partners

Magnetic cooling, if enabled by a cost-efficient approach that is underpinned by the minimal use and wastage of rare earths, will help EC member states to reach carbon emission targets. Again, our finding that the rare earth use of an A+++ domestic refrigerator could be reduced by 74% should help greatly in this direction.

### 4.1.3 Support to EU policies

Our work on magnetic cooling supports EU policies in several ways:

Firstly, the implementation of the European Union's WEEE (Waste Electrical and Electronic Equipment) and RoHS (Restrictions on the Use of Certain Hazardous Substances) directives requires cooling engine manufacturers to examine their current systems and look for alternatives with a lower environmental impact over the complete lifetime of the product. The net effect is that solid state cooling technology is attracting interest from all sectors and our work will enable manufacturers to comply with these regulations. The commitment of Indesit to this proposal demonstrates the prospects for magnetic cooling to satisfy WEEE and RoHS directives in the near future.

Secondly, as described in Section 1, European Union directive EC C(2010) 6481 bans all domestic fridges lower than class A, and **created a new high-efficiency A+++ class from late 2011**. Consumer demand and the efficiency advantages of magnetic cooling will enable this directive to be followed.

Finally, REACH is the European Community Regulation on chemicals and their safe use (EC 1907/2006) and deals with the Registration, Evaluation, Authorisation and Restriction of Chemical substances. Its aim is to improve the protection of human health and the environment through the better and earlier identification of the intrinsic properties of chemical substances. Our LCA of the magnetic refrigerator will be conducted in the context of this regulation and will be compared with the results of LCA on gas compression-based refrigerators.

Our research should therefore have impacts in the following areas, which are listed according to categories (i-iv) in the call fiche:

(i) Innovative magnetocaloric materials applications, principally magnetic cooling, will become scalable for the first time and brought to a cost point for entry into suitable markets. Energy savings will result from mass adoption of these technologies.

(ii) Magnetocaloric materials will be produced by a less wasteful route, and will therefore be less reliant on the critical raw material constituent(s). Magnetocaloric materials with zero rare earth content will be studied in tandem.
(iii) Through life cycle analysis of our product chain, we will reduce the reliance of the magnetocaloric sector on fresh supplies of rare earth metals and oxides.
(iv) Our partnership has actively promoted rare earth-conserving approaches to alloy design, production and device implementation, and supports the development of a European Competence Network on Rare Earths, as suggested by the Öko Institute [2].
(v) Our studies of compostionally graded magnetic thin films will provide insight in the parallel research area of energy harvesting by multi-functional micro-systems.

### 4.1.4 Technological and commercial impact

The European refrigeration and heat pumping industries, which include leading companies, such as Electrolux, Bosch, Clivet and Indesit, directly employ hundreds of thousands of people across Europe, and indirectly provide employment for hundreds of thousands more. However the industry is facing the twin challenges of needing to be more environmentally friendly and low cost competition from outside Europe.

From this perspective the technology and commercial objective of this project have been to:

- Focus on development of novel clean technologies in the energy conversion space that will:
  - Reduce energy consumption by virtue of being more efficient
  - Ensure a technology that is easy to recycle by eliminating gas refrigerants and replacing them with components that are desirable to recycle such as magnets and solid refrigerants.
  - Reduce maintenance costs by eliminating gas leaks
  - Provide an innovation led response by the industry to legislative and overseas competition pressures.

Market demand for this solution is clear:

- Consumers wish to adopt this technology to reduce their individual carbon footprints, and to save money.
- Commercial users have over the last 15 years, and for the foreseeable future, have had to make a series of capital investments in new technologies to move from CFC to HFC and now to CO2-based systems. There is a demand for a non-gas based solution that is robust against environmental legislation.
- In certain industries (e.g. railways) gas based cooling options are no longer viable; a solid state solution is effectively being mandated by legislation.

In summary, this project has aimed to have a positive impact on jobs, the environment, competitiveness and European innovation.

## 4.2 Main dissemination / exploitation of results

Magnetic cooling is one of several **interdisciplinary ferroic cooling** research areas (including the parallel fields of mechanocaloric and electrocaloric cooling) that are the subject of increased interest within the physics, materials science and engineering research communities and from refrigeration industries and the general public.

We have exploited many different forms of dissemination, a list of which is given in section A, “Use and dissemination of foreground” of our SESAM submission accompanying this document. At the time of writing, a total of **over 120 separate acts of dissemination** have been carried out, ranging from journal publications, oral and poster presentations at conferences, invited seminars at various institutions across the world, media interviews, magazine articles and articles in the popular press. This number will continue to grow in the coming months as scientific results from the project are published in peer-reviewed journals.

A summary of our dissemination activities under relevant headings is now presented.

*Journal articles*
During the course of the project (January 2013 – December 2015) we have published **13 peer-reviewed journal articles in high impact journals** such as *Advanced Energy Materials* and *Europhysics Letters*. Many of these involve co-authorship by two or more project partners, highlighting the degree of interaction within our consortium. Since the conclusion of the project another **9 peer-reviewed journal articles** have followed. The total of **22 journal articles** thus far will continue to grow in the coming months.

*Conference presentations*
The visibility of magnetocaloric materials and magnetic cooling research has greatly increased during the project, in no small way due to the activities of the consortium partners. Members of the consortium gave **over 54 invited or contributed presentations** at national or international conferences. Consortium members chaired symposia on magnetocaloric materials at several conferences, including at ICM, MMM and MMM-Intermag 2016. The DRREAM project has been, or will be, presented at interdisciplinary meetings on caloric materials in: Germany (DFG "Ferroic Cooling" Priority Programme 1599 project meeting, December 2013), the UK (Winton Meeting on Caloric Materials, February 2016) and in the US (AMEC Workshop, April 2015 and the Spring MRS meeting, March 2016).

*Invited presentations*
During the course of the project a total of **28 invited presentations** were given by partners at large-scale conferences, focussed workshops and national project meetings across the world. Many of these were given in Europe, the USA or Canada. DRREAM partner Oliver Gutfleisch gave a plenary address to the MMM-Intermag 2016 conference on "Magnets for Energy Conversion and Heating" in January 2016. DRREAM was also featured in a session on magnetic materials projects funded by the EU at the JEMS 2013 meeting.

*Magazine articles*
The application of magnetic cooling to different market sectors continues to attract interest from general media and industry-led journals. The coordinator co-wrote an article on solid-state cooling for *Physics Today*, the magazine of the American Institute of Physics. It was the cover article for December 2015. One other piece was published in *Magnetics Technology International.*

# 5. Project website and contact details

The project website is http://www.drream.eu. Both route to the same set of webpages. The website has attracted over 3200 visitors since tracking statistics were first collected in January 2013. 70% of visitors are from Europe, 16% from the USA and 4% from Asia. The website also acted as a central resource for partners to share key information, via a private area.

Contact details for the 8 consortium partners are given below.

**1. Imperial College (coordinator)**
Dr. Karl Sandeman
EXSS Group, Department of Physics
Imperial College London
Prince Consort Road
London SW7 2AZ
United Kingdom
Email: k.sandeman@imperial.ac.uk
Tel: +44 207 290 9182
Fax: +44 207 594 2077

**2. TU Darmstadt**
Dr. Oliver Gutfleisch
Institut für Materialwissenschaft
FG Funktionale Materialien
Technische Universität Darmstadt
Petersenstr. 23
64287 Darmstadt
Germany
Email: gutfleisch@fm.tu-darmstadt.de
Tel: +49 6151 16-75559
Fax: +49 6151 16-72559

**3a. CNRS SATIE/ICMPE**
Dr. Martino Lo Bue
ENS de Cachan 61
Avenue du Président Wilson
94235 Cachan
France
Email: Martino.LO-BUE@satie.ens-cachan.fr
Tel: +33 1 47 40 74 89
Fax: +33 1 47 40 21 99

**3b. CNRS Institut Néel**
Dr. Nora Dempsey
Institut Néel (CNRS & UJF) - Building D
25 rue des Martyrs
BP166 - 38042 Grenoble
France
Email: nora.dempsey@neel.cnrs.fr
Tel: +33 1 47 68 87 435
Fax: +33 1 47 68 81 191

**4. INRIM**
Dr. Vittorio Basso
Istituto Nazionale di Ricerca Metrologica
Strada delle Cacce 91
10135, Torino
Italy
Email: basso@inrim.it
Tel: +39 011 3919 842
Fax: +39 011 3919 834

**5. Fraunhofer IFAM**
Dr. Thomas Studnitzky
Cellular Metallic Materials
Fraunhofer IFAM Dresden
Winterbergstraße 28
01277 Dresden
Germany
Email: thomas.studnitzky@ifam-dd.fraunhofer.de
Tel: +49 351 2537 339
Fax: +49 351 2554 465

**6. Indesit**
Mehmet Acar
Indesit Company SpA
Viale Aristide Merloni 47
60044 Fabriano (AN)
Italy
Email: mehmet.acar@indesit.com

**7. Vacuumschmelze GmbH & Co. KG**
Dr. Alexander Barcza
Vacuumschmelze GmbH & Co. KG
Grüner Weg 37
D-63450 Hanau
Germany
Email: alexander.barcza@vacuumschmelze.com
Tel: +49 6181 38-2161
Fax: +49 6181 38-82161

**8. Camfridge Ltd.**
Dr. Neil Wilson
Copley Hill Business Park
Lower Court 1
Babraham Road
Babraham
Cambridge
CB22 3GN
United Kingdom
Email: nwilson@camfridge.com
Tel: +44 7903 502329